ISTANBUL TECHNICAL UNIVERSITY ★ GRADUATE SCHOOL OF SCIENCE ENGINEERING AND TECHNOLOGY

CATALYSIS OF ATP HYDROLYSIS BY THE CHAPERONE PROTEIN HSP70

M.SC THESIS

Oğuzhan MARABA

Department of Molecular Biology Genetics and Biotechnology

Molecular Biology Genetics and Biotechnology Program

DECEMBER 2015

ISTANBUL TECHNICAL UNIVERSITY ★ GRADUATE SCHOOL OF SCIENCE ENGINEERING AND TECHNOLOGY

CATALYSIS OF ATP HYDROLYSIS BY THE CHAPERONE PROTEIN HSP70

M.SC THESIS

Oğuzhan MARABA
(521131116)

Department of Molecular Biology Genetics and Biotechnology

Molecular Biology Genetics and Biotechnology Program

Thesis Advisor: Assist. Prof. Dr. Bülent BALTA

DECEMBER 2015

İSTANBUL TEKNİK ÜNİVERSİTESİ ★ FEN BİLİMLERİ ENSTİTÜSÜ

ATP HİDROLİZİNİN HSP70 ŞAPERON PROTEİNİ TARAFINDAN KATALİZLENMESİ

YÜKSEK LİSANS TEZİ

Oğuzhan MARABA
(521131116)

Moleküler Biyoloji Genetik ve Biyoteknoloji Anabilim Dalı

Moleküler Biyoloji Genetik ve Biyoteknoloji Programı

Tez Danışmanı: Yrd. Doç. Dr. Bülent BALTA

ARALIK 2015

Oğuzhan MARABA, a M.Sc. student of ITU Graduate School of Science, Engineering and Technology, student ID 521131116 successfully defended the thesis/dissertation entitled "CATALYSIS OF ATP HYDROLYSIS BY THE CHAPERONE PROTEIN HSP70" which he prepared after fulfilling the requirements specified in the associated legislations, before the jury whose signatures are below.

Thesis Advisor :	**Assist. Prof. Dr. Bülent BALTA** İstanbul Technical University	.....
Jury Members :	**Assoc. Prof. Dr. Gizem DİNLER DOĞANAY** İstanbul Technical University	.....
	Assist. Prof. Dr. Şaron ÇATAK Boğaziçi University	.....

Date of Submission : 27 November 2015
Date of Defense : 23 December 2015

FOREWORD

I would like to thank my advisor, Assistant Professor Bülent Balta for his continious assistance during my internship back in 2011 and during my M.Sc. education. If not for him, I don't think I would be interested in computational chemistry and pursue a career in this field. It was a great experience for me to study with him.

I would also like to thank my friends in our research group, Aydın Özmaldar and Ayla Başaran Kınalı, my friends in MOBGAM and my family for their support.

December 2015

Oğuzhan Maraba
Biochemist

TABLE OF CONTENTS

Page

FOREWORD ..... **vii**
TABLE OF CONTENTS ..... **ix**
ABBREVATIONS ..... **xi**
LIST OF TABLES ..... **xiii**
LIST OF FIGURES ..... **xv**
SUMMARY ..... **xvii**
ÖZET…… ..... **xix**
1. INTRODUCTION **1**
1.1 Biological Role of the Hsp70 1
1.2 Structure and Functional Cycle of the Hsp70 2
1.3 Active Site of Hsp70 and Mutation Studies 5
1.4 General Mechanisms For Phosphate Hydrolysis 8
1.5 Suggested Mechanisms 10
1.6 Aim of the Study 11
2. MATERIALS AND METHODS **13**
2.1 Density Functional Theory 14
2.2 Basis Set 23
2.3 ONIOM 25
2.4 MM Force Fields 26
3. RESULTS AND DISCUSSION **29**
3.1 Hydrolysis in the 201N System 29
3.2 Hydrolysis in the 201I System 38
4. CONCLUSIONS AND RECOMMENDATIONS **47**
REFERENCES **49**
CURRICULUM VITAE **53**

ABBREVATIONS

201I	**:**Models with ionized D201
201N	**:**Models with neutral D201
AcidWI	**:**Water between two ions as an acid in the model with ionized D201
AcidWN	**:**Water between two ions as an acid in the model with neutral D201
ATP	**:**Adenosine triphosphate
ADP	**:**Adenosine diphosphate
Bij	**:**Coulomb potential
CI	**:**Crystal-like product structure for the model with ionized D201
cc-PVNZ	**:**Correlation-consistent Polarized Valence N-Zeta
D	**:**Number of atoms in the system
D	**:**Aspartic acid
DFT	**:**Density Functional Theory
E	**:**Potential energy
E	**:**Glutamic acid
Eb	**:**Energy for bond angle
Enb	**:**Energy for non-bonded interactions
Es	**:**Energy for bond stretching
Eω	**:**Torsional energy
E_{xc}	**:**Exchange-correlation Potential
G	**:**Glycine
GGA	**:**Generalized Gradient Approximation
GTO	**:**Gaussian Type Orbitals
$\hat{H}$	**:**Hamiltonian operator
HF	**:**Hartree-Fock
K	**:**Lysine
K	:Exchange integral
KS	:Kohn-Sham
k_b	**:**Force constant for bending
k_s	**:**Force constant for strectching
LCAO	**:**Linear Combination of Atomic Orbitals
LDA	**:**Local Density Approximation
l	**:**Actual bond length
l_0	**:**Assigned bond length
M	**:**Total number of bond angles
m	**:**Mass
N	**:**Total number of bonds
P	**:**Proline
P171I	**:**Product structure with a proton passed to E171 in the model with ionized D201
P201I	**:**Product structure with a proton passed to E171 in the model with ionized D201
PCM	**:**Polarized Continuum Model
PHI0	**:**Reference product with a deleted proton from Pi in the model with ionized D201
PHI1	**:**First alternative product model with a deleted proton from Pi in the model with ionized D201

PHI2 **:**Second alternative product model with a deleted proton from Pi in the model with ionized D201
PI **:**Product structure for the model with ionized D201
Pi **:**Inorganic phosphate
PN **:**Product structure for the model with neutral D201
R **:**Arginine
RI **:**Reactant structure for the model with ionized D201
RN **:**Reactant structure for the model with neutral D201
RMgN **:**Reactant structure with magnesium ion between two phosphate groups in the model with netutral D201
q **:**Phase point
q_i **:**Partial charge on atom i
q_j **:**Partial charge on atom j
r_{ij} **:**Distance between atoms i and j
S **:**Serine
SCRF **:**Self-Consistent Reaction Field
SMD **:**Solvation Model –Density
STO **:**Slater Type Orbitals
T **:**Threonine
T **:**Absolute temperature
TS **:**Transition state
TSN1 **:**First alternative for the transition state of the 201N model
TSN2 **:**Second alternative for the transition state of the 201N model
TSN3 **:**Third alternative for the transition state of the 201N model
Ψ **:**Many electron wavefunction
χ_i **:**One-electron orbital
γ **:**Phase factor
ε **:**Dielectric constant of medium
θ **:**Actual bond angle
θ_0 **:**Assigned bond angle
$\lambda(k)$ **:**Step size
ω **:**Torsion angle

LIST OF TABLES

Page

Table 3.1 : Relative energies (with respect to RN) of the stationary points in the reaction of 201N. 29
Table 3.2 : Relative energies (with respect to RI) of the stationary points in the reaction of 201I 38
Table 3.3 : Relative energies (With respect to PHI0) of the stationary points in the reaction of 201I. 43

LIST OF FIGURES

Page

Figure 1.1 : Structure of Hsp70. 3
Figure 1.2 : Functional Cycles of Hsp70 4
Figure 1.3 : pH profile of Hsp70 5
Figure 1.4 : D206S Mutant Crystal Structure of Bovine Hsc70 6
Figure 1.5 : A schematic description of the potential surface for the hydrolysis of Phosphomonoesters 9
Figure 2.1 : The components of the ONIOM scheme 26
Figure 2.2 : Force field elements. 27
Figure 3.1 : The most stable reactant structure (RN) in the 201N system. 30
Figure 3.2 : Alternative reactant structure (RMgN). 31
Figure 3.3 : The most stable product structure (PN) in the 201N system. 32
Figure 3.4 : The associative transition state (TSN1) 33
Figure 3.5 : The associative transition state (TSN2) 34
Figure 3.6 : Associative transition state (TSN3) 35
Figure 3.7 : The water between Mg^{2+} and K^{+} as an acid (AcidWN). 37
Figure 3.8 : Energy versus reaction path graph of the 201N models 38
Figure 3.9 : The most stable reactant structure (RI) in the 201I system. 39
Figure 3.10 : The most stable product structure (PI) in the 201I system. 40
Figure 3.11 : The product with E171 accepting a proton from Pi (P171I). 40
Figure 3.12 : The product with D201 not accepting a proton from Pi (P201I). 41
Figure 3.13 : The Product with ATP+Mg obtained from crystal structure (CI). 42
Figure 3.14 : Reference product with a deleted proton from Pi (PHI0) 43
Figure 3.15 : First product with a deleted proton on Pi (PHI1) 44
Figure 3.16 : Second product with a deleted proton on Pi (PHI2) 45
Figure 3.17 : The water between Mg^{2+} and K^{+} as an acid (AcidWI) 46
Figure 3.18 : Energy versus reaction path graph of the 201I models 46

CATALYSIS OF ATP HYDROLYSIS BY THE CHAPERONE PROTEIN HSP70

SUMMARY

Molecular chaperone proteins assist the newly synthesized proteins to fold into the native structure. Many chaperone proteins are also heat shock proteins, which assists refolding of the proteins denatured under stress conditions, with Hsp70 being one of them. Besides being a heat shock protein, Hsp70s are also responsible for the membrane translocation of secretory and organellar proteins and controlling the activity of regulatory proteins. Co-chaperones and/or cooperation with other chaperone systems are needed for these pathways.

In this study, the ATP hydrolysis mechanism of Hsp70 has been investigated using the QM/MM ONIOM method with M06-2X for the QM part and the AMBER force field for the MM part. Two main models were created (which are decided with respects to the results of our group's previous study) depending on the protonation states of D201.

Particular attention has been paid to the role of K70 as it is known experimentally that this residue is crucial for ATP hydrolysis. Geometry optimizations have been carried out on structures where this residue is coordinated to the nucleophilic water or oriented away from this water. In addition, the possibility that K70 is involved in acid catalysis has been investigated.

Other acid-base catalysis options were also considered with D194 and a water molecule between Mg2+ and K+ also being an acid candidate and E171 as a base candidate.

In general, phosphate hydrolysis reactions can take place either through an associative or a dissociative mechanism depending on the environment. Therefore, both mechanisms are tested in order to identify lowest energy pathway.

In the crystallographic structure, a Mg2+ ion is coordinated to the beta-phosphate group. In the literature, it is suggested that the reaction begins by the shift of this Mg2+ to a position between the beta- and gamma-phosphate groups. Therefore, both positions of Mg2+ have been considered in QM/MM geometry optimizations.

Our results showed that proton transfer to ATP occurs with nucleophilic water directly attacking the ATP and acid-base catalysis does not seem to be an option for ATP hydrolysis in Hsp70. The shift of Mg2+ between the two phosphate groups is also energetically unfavorable.

On the other hand, in the models with a deprotonated D201, Pi tends to donate a proton to a nearby water or E171, which suggests that E171 can accept a proton after product formation. And when a proton is deleted on Pi, Mg2+ shift between the two phosphate groups is energetically favorable.

ATP HİDROLİZİNİN HSP70 ŞAPERON PROTEİNİ TARAFINDAN KATALİZLENMESİ

ÖZET

Proteinler katlanmamış polipeptidler veya rastgele sarmallar halinde sentezlenirler. Biyosentezin tamamlanmasından sonra bu yapılar aminoasit sekanslarının belirttiği şekilde üç boyutlu yapılarına katlanırlar. Bir proteinin doğal üç boyutlu yapısına katlanması protein olarak işlev görmesi için gereklidir. Proteinler doğru üç boyutlu yapılarına katlanamazlarsa inaktif yapıda bulunurlar. Yanlış katlanmış bu yapılar çökelebilirler, farklı fonksiyonlara sahip olabilirler ya da hücre içinde zararlı bir etki oluşturabilirler. Örneğin, bazı nörodejeneratif hastalıklar yanlış katlanmış proteinler nedeniyle meydana gelmektedir.

Proteinler kendilerini hücre ortamının kalabalıklığına rağmen kendi kendilerine katlayabilirler. Ancak diğer moleküllerle meydana gelen etkileşimler yanlış katlanmalara sebebiyet verebilir. Moleküler şaperon proteinleri yeni sentezlenmiş proteinlerin doğal yapılarına katlanmalarında onlara yardımcı olur. Şaperon proteinlerinin çoğu aynı zamanda ısı-şok proteinidir. Bu proteinler stres koşullarında denatüre olmuş proteinlerin yeniden katlanmasına yardım etmede görev almaktadır. Hsp70 de bu proteinlerden bir tanesidir. Isı-şok proteini olmasının yanı sıra, Hsp70 proteinleri regülatör proteinlerin aktivitesinin kontrolünü, organelve salgı proteinlerinin membran translokasyonundan da sorumludur.

Hsp70, 45 kDa N-uç ATPaz domain ve 25 kDa C-terminal substrat bağlanma domaini içeren 70 kDalık bir proteindir. ATPaz domain ve substrat bağlama domaininin arasında bir bağlaç sekansı bulunur. Bu bağlaç allosterik iletişimde görev alır.

Hsp70'de ATP hidrolizi iki ana hali içeren bir döngü şeklindedir. ATP bağlı olduğu durumda substrat afinitesi düşüktür. Bağlı ATP hidrolizlenip ADP ve Pi oluştuğunda ise substrata olan afinite artış gösterir.

Hsp70'in ATP hidroliz mekanizması ile ilgili yapılan çalışmalar genellikle aktif merkez içindeki bir ya da birkaç aminoasidin mutasyona uğratılmasıyla bu aminoasitlerin hidrolize etkisi araştırılarak hidroliz reaksiyonu için esansiyel olup olmadıklarının araştırılmasına yöneliktir.

Bu çalışmada Hsp70'in ATP hidroliz mekanizması QM/MM ONIOM methoduyla QM bölge için M06-2X, MM bölge için AMBER kuvvet alanı kullanılarak incelenmiştir. Grubumuzda daha önceden yapılan moleküler dinamik simülasyonlarına dayanarak 201. Pozisyondaki aspartik asidin protonasyon durumlarına göre iki ana model düşünülmüştür. Bu modellerin tasarımında ilgili moleküler dinamik simülasyonundan alınmış anlık bir görüntüden faydalanılmıştır.

Önceki çalışmalarda hidroliz için kritik bir aminoasit olduğu bulunan K70'in üzerinde özellikle durulmuştur. Nükleofilik suya olan mesafesine göre çeşitli geometriler hazırlanıp optimize edilmiştir. Ek olarak, K70'in asit-baz katalizine girip girmediği de araştırılmıştır. Bununla birlikte, asit-baz katalizinde rol oynayabileceği düşünülen başka aminoasitlerle de asit-baz katalizi reaksiyonlarını ifade eden modeller hazırlanmıştır. Asit adayı olarak K70'in yanı sıra, D194 ve Mg2+ ile K+ arasında bulunan bir su molekülü düşünülmüş, baz olarak ise E171 seçilmiştir.

ATP hidroliz mekanizmaları asosiyatif veya disosiyatif olarak gerçekleşmektedir. Mekanizmanın hangi yönde gerçekleşeceği reaksiyonun meydana geldiği ortama bağlıdır. Bu nedenden dolayı iki mekanizma da test edilmiştir.

Kristallografik çalışmalarda ATP'ye koordine olmuş bir Mg2+ iyonunun beta fostat grubu ile etkileştiği gözlemlenmiştir. Literatürde bu iyonun beta ile gamma fosfatın arasına kaymasıyla reaksiyonun başlayabileceği öne sürülmüştür. Bunu test etmek amacıyla bu iyonun farklı pozisyonda olduğu geometriler ele alınmıştır.

201. Pozisyondaki aspartik asidin iyonize ve nötral halde bulunduğu yapılardan alınan başlangıç geometrilerinin optimizasyonundan sonra öncelikle hidrolizin olduğu ilk anı ifade eden ürün yapıları türetilmiştir. Daha sonra sonuçların gösterdiği doğrultuda aktif merkezin içinde olabilecek farklı durumlar tasarlanıp modellenmiştir.

Sonuçlanan çalışmalarda, D201'in nötral olduğu yapılarda ATP hidroliz mekanizmasının nükleofilik suyun doğrudan saldırısıyla gerçekleştiği görülmüştür. Ortaya çıkan geçiş hali yapısı ise asosiyatif karakterlidir. Bununla birlikte asit-baz katalizi içeren çalışmalar enerjetik olarak uygun sonuçlar vermemişlerdir. Mg2+ iyonunun iki fosfat grubu arasına kaydığı çalışmalarda ise bu iyonun arada durduğu yapılar ya başlangıç geometrilerine geri dönmüştür, ya da rölatif olarak çok yüksek enerjili sonuçlar vermişlerdir.

Diğer yandan, D201'in iyonize olduğu durumlardaki yapılarda Pi'ın proton verme eğiliminde olduğu görülmektedir. Bu çalışmanın sonucunu gözlemledikten sonra Pi'dan E171 ve D201'e proton geçişini ifade eden yapılar optimize edilmeye çalışılmıştır. Bu optimizasyonların sonucunda D201'in protonu kabul etmeyip suya geri göndererek hidryonyum oluşturduğu, E171'in ise protonu kabul ettiği görülmüştür. Bu iki sonuç birbirine eş rölatif enerjili çıkmıştır.

Mg2+ iyonu bu iş setinde de iki fosfat iyonunun arasına kaydırılmış, ancak diğer iş setinde olduğu gibi olumlu bir sonuç alınamamıştır.

Sistemde hidronyum oluşması, bu hidronyumun ortamı terk edebilme ihtimalinin, yani ortamdan Pi'dan gelen bir hidrojenin ortadan kaybolduğu bir halin gözden geçirilmesini sağlamıştır.

Bir hidrojenin ortamdan uzaklaştırıldığı durumu tespit etmek amacıyla öncelikle bir referans model oluşturulmuştur. Bu modelde Pi'ın önceki çalışmalarda suya proton verip hidronyum oluşturduğu hidrojen manuel olarak silinmiştir. Bu geometrinin optimizasyonundan sonra biri bu referans alınacak geometrideki aynı hidrojen, diğeri de hidroliz reaksiyonu sırasında Pi'ın aldığı diğer Hidrojen olmak üzere iki farklı hidrojen atomundan birinin silindiği iki geometri oluşturulup optimize edilmiştir. Bu geometrilerde Mg2+ ADP ile Pi arasına yerleştirilmiştir.

Optimizasyonlar sonuçlandığında bu iki geometrinin de Mg2+ iyonunun sadece ADP ile etkileştiği referans geometrisinden daha düşük enerjili olduğu sonucu bulunmuş, bu iki geometriden de hidroliz sırasında gamma fosfata verilen hidrojenin silindiği geometrinin daha düşük enerjiye sahip olduğu gözlemlenmiştir.

1. INTRODUCTION

Hsp70 is an allosterically regulated chaperone protein which consists of an ATPase domain and a substrate binding domain connected by a conserved linker, which mediates the allosteric communication between two domains. The affinity of Hsp70 to substrates, which are misfolded proteins, is low when ATP is bound. Upon substrate binding, ATP is hydrolyzed into ADP and the affinity to the substrate increases [1]. Although several mechanisms are suggested, how ATP is hydrolyzed is still unclear. There are still unanswered questions about the position of the linker or the roles of the residues like K70 which is essential for ATPase domain to function. The reaction also shows pH dependency with the optimum pH being 7.5 [2]. There are ionizable amino acids in or near the active site (E171, D194 and D201) and their protonation states may be important for the reaction. There is a Mg^{2+} ion, its shift between β- and γ-phosphate is thought to initiate the reaction[3]. The hydrolysis mechanism itself is also unknown, which can be either associative or dissociative depending on the environment. This study focuses on the *E. coli* Hsp70 homolog DnaK in order to contribute to the understanding of the ATPase mechanism in this protein.

1.1 Biological Role of the Hsp70

Proteins are synthesized as unfolded polypeptides or random coils. After biosynthesis, they fold into their native structure dictated by their amino acid sequence. Native three dimensional structure is important for polypeptides to function as a protein. If a protein does not fold into its correct three dimensional structure, this will result in an inactive protein. These misfolded proteins can be aggregated, have modified functionality or can be harmful for the cells. For example, several neurodegenerative diseases can be caused by misfolded proteins.

Although a protein can fold correctly by itself, in the crowded cellular environment, interactions with other molecules may lead to misfolding. Molecular chaperone proteins assist the newly synthesized proteins to fold into their native structure. Many

chaperone proteins are also heat shock proteins, which assist refolding of the proteins denatured under stress conditions, Hsp70 being one of them. Besides being a heat shock protein, Hsp70s are also responsible for the membrane translocation of secretory and organellar proteins and controlling the activity of regulatory proteins. Co-chaperones and/or cooperation with other chaperone systems are needed for these pathways.

Hsp70s can either assist folding a newly synthesized protein into the native structure, preventing aggregation or refolding an aggregated protein depending on a given situation. Mechanism of folding a substrate into its native structure is still unclear, but there are two suggested mechanisms. One involves repetitive binding and releasing the substrate. This makes the concentration of free unfolded proteins lower. With the low concentration, it is possible to prevent aggregation and the free molecules will fold into their native state. The second mechanism involves local unfolding of the misfolded parts of the substrate to overcome kinetic barriers for refolding. J-domain proteins, which are co-chaperones, help prevention of aggregation by binding to the unfolded parts of the substrates. The J-domain proteins bind to the substrate and chaperone simultaneously. With their help, the molecular chaperone system interacts with the hydrophobic residues in the substrate. This interaction of the system with the substrate prevents intermolecular interactions of the substrate. Solubilization of the aggregates can be possible with cooperation from Hsp100 chaperones by some Hsp70s [1].

1.2 Structure and Functional Cycle of the Hsp70

Heat-shock protein 70 is 70 kDa. It consists of a 45 kDa N-terminal ATPase domain and a 25 kDa C-terminal substrate binding domain. The ATPase domain has two subdomains named A and B, both of which can be divided into subdomains I and II. The substrate binding domain is also divided into a beta-sandwich subdomain and an alpha-helical subdomain (Figure 1.1). There is a linker sequence between the ATPase domain and the substrate binding domain to mediate allosteric communication. Crystallography studies show that the nucleotide binds in the cleft between the subdomains I and II. ATP binding as well as the release of the ADP and Pi is possible with the conformational changes of these two subdomains of the ATPase domain.

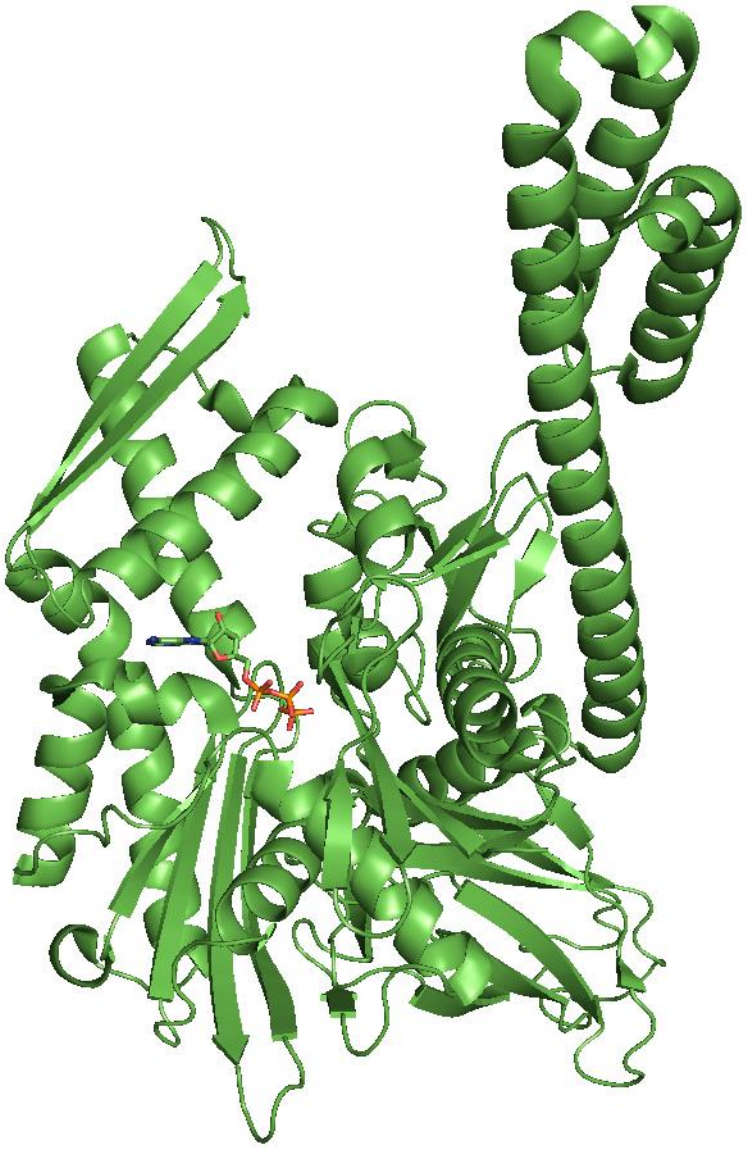

Figure 1.1 : Structure of Hsp70 [4].

ATP hydrolysis in Hsp70 is a cycle involving two main states: When ATP is bound, substrate affinity is low. When the ATP is hydrolysed into ADP + Pi, substrate affinity is high.

In the ATP state, the ATP binding cleft between the subdomains I and II is more closed than in the ADP state, and the binding cavity in the substrate binding domain is open. In this state, the two domains are docked onto each other. The helical subdomain of SBD is bound to subdomain I of NBD. Thus, it is oriented away from the rest of SBD and does not close the substrate binding site.

Hydrolysis rate of the DnaK in the ground state ranges between 3.10^{-4} to $1.6.10^{-2}$ s^{-1}, which is very low. ATP hydrolysis reaction can be stimulated by the substrate by 2 to

10 fold, which is also very low to have properly functioning cycles. J-domain co-chaperone proteins are needed to overcome this situation. *Escherichia coli* J-domain protein member, named DnaJ, stimulates the rate of ATP hydrolysis to an extent similar to the substrate. However, the substrate and DnaJ together stimulate the rate synergistically by higher than 1000 fold. This mechanism involves DnaJ binding the ATPase domain and the substrate protein simultaneously [1].

In the state with ATP and the substrate are bound at the same time (Figure 1.2), the conformation either leads to ATP hydrolysis or substrate dissociation. System decides which way to go with both intermolecular interactions between two domains and between the bound substrate and the co-chaperones [5].

In the ADP state, the two domains separate from each other. This movement releases the helical subdomain of SBD (from subdomain I) which closes the substrate binding cavity. The dissociation rate of the ADP is very low, 0.0004-0.0014 s^{-1}. If Pi is also in the environment, dissociation rate is 0.004-0.035 s^{-1}. The low ADP release rate, together with the increase in the substrate affinity, provides the necessary time for folding [1].

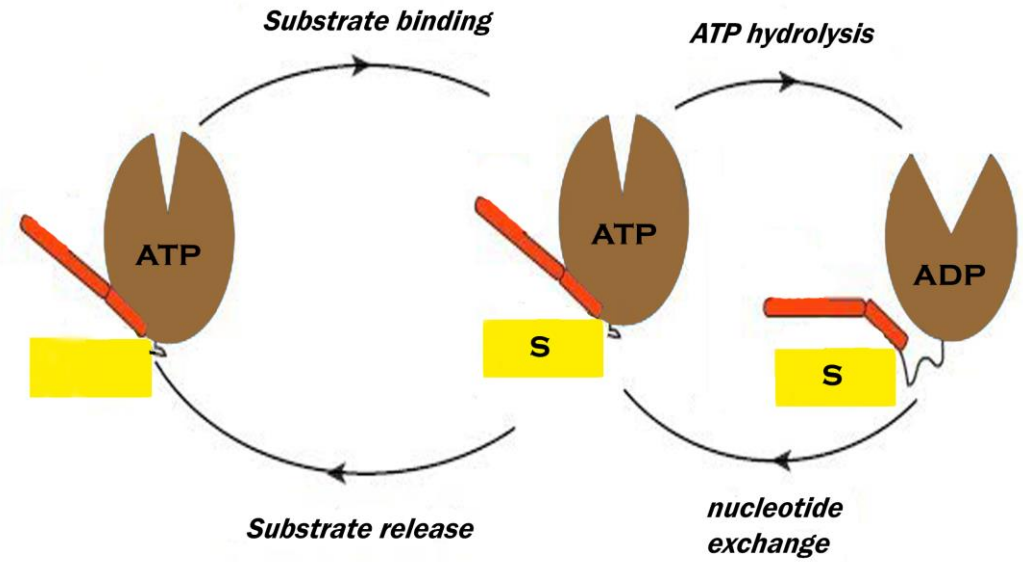

Figure 1.2 : Functional Cycles of Hsp70 [5].

The release of ADP is accelerated by the nucleotide exchange factors (GrpE for *Escherichia coli* DnaK). In the presence of GrpE, the nucleotide binding cleft in the

ATPase domain opens up to allow the dissociation of ADP. Next, ATP binds to restart the cycle.

In the studies with only the NBD domain, two structures, one with the linker sequence (1-392) and one without the linker (1-388) were used to see if there is a difference between them. The results show that the NBD construct with the linker sequence has the same ATPase rate with the full length protein that also has a substrate, but the other construct (1-388) has the same rate with the full length protein without a substrate.

ATP hydrolysis reaction shows a bell-shaped pH dependence when substrate is present, with the highest ATPase rate seen at pH 7.5. In contrast, in the absence of the substrate, no pH dependence was observed. (1-388) construct replicates the same result with this, whereas (1-392) constructs show a bell shaped pH profile (Figure 1.3)[2].

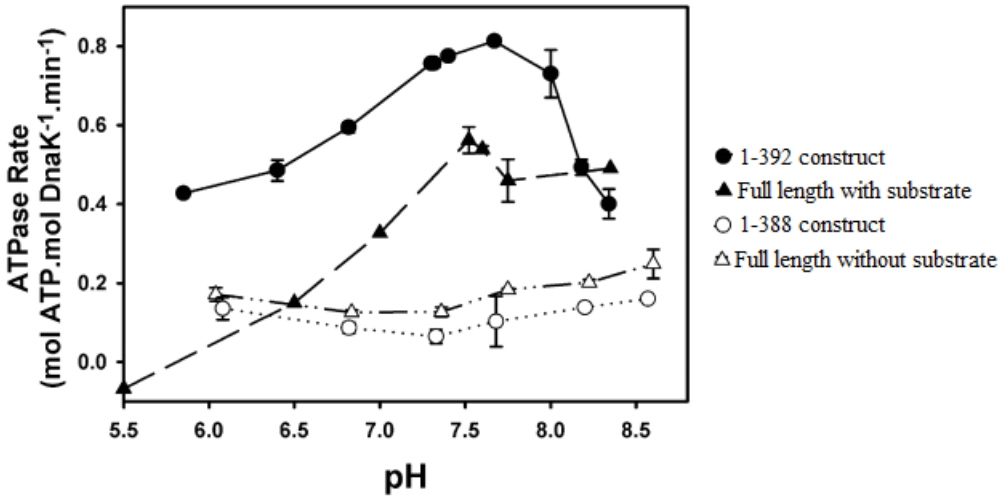

Figure 1.3 : pH profile of Hsp70 [2].

1.3 Active Site of Hsp70 and Mutation Studies

Figure 1.4 shows ADP+Pi bound bovine Hsp70 homolog Hsc70 crystal [6]. The nucleotide is bound in the cleft between the two subdomains I and II. A Mg^{2+} ion is coordinated between Pi and the β-phosphate group of ADP. Mg^{2+} also interacts with 4 nearby waters to create an octahedral coordination shell. There are also two K^{+} ions in the environment. One is coordinated between Pi, β-phosphate group of ADP and T199. The other one is coordinated between D8 and β-phosphate group of ADP.

Without the K^+ ions in the environment, Mg-ATP binding does not induce substrate dissociation. This experiment is also done with Na^+ instead of K^+ and Na^+ ions could not replace the function of K^+ ions. Studies also show that the steady state ATPase activity is stimulated by monovalent cations and the turnover rate changes with the ionic radius of the cation in the environment. When Na^+ is present in the environment instead of K^+, steady state ATPase rate was 10-fold slower, whereas NH_4^+ or Rb^+ addition halves the observed turnover rate with K^+ [7,8,9].

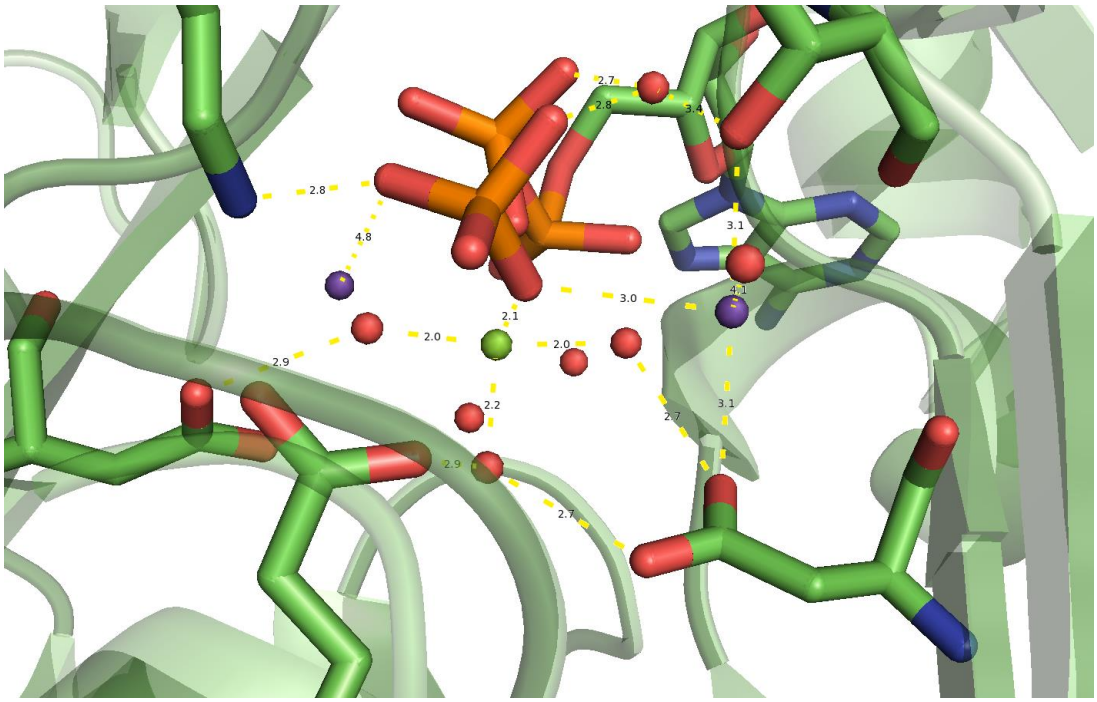

Figure 1.4 : D206S Mutant Crystal Structure of Bovine Hsc70 [6].

K70, E171, T12 and T199 possibly interact with the Pi directly with a hydrogen bond. T199 is also an autophosphorylation site. D201 interacts with a water molecule interacting with Pi. D8 and E171 interact with a water molecule in the coordination shell of Mg^{2+}.

Mutation studies give insight to the pH dependency of the ATPase domain. When D194 is mutated into alanine in the DnaK(1-392) construct, instead of a bell-shaped activity profile, the ATPase activity increases with the increasing pH. Mutating E171 and D201 to alanine in the DnaK(1-392) construct made Hsp70 lose its ATPase activity, so commenting on the pH dependency was not possible [10].

When these mutations were done in an ATPase domain construct with no linker sequence (DnaK(1-388)), the wild type and the mutants did not show pH dependency but all of the mutants had higher ATPase activities than the wild type.

When T199 was mutated into alanine, ATPase and autophosphorylation activities were lost, but the T199S mutation resulted in near wild-type level of steady state rate and the observed autophosphorylation activity was 13 percent of the wild type. With these results, it is thought that the autophosphorylation is not an obligatory reaction in the ATP hydrolysis process. Mutation of the corresponding residue in bovine homolog Hsc70 (T204) into valine and glutamic acid resulted in increased K_m values for ATP (1 to 90 μM).

K70 is found to be an essential residue for the ATP hydrolysis in the studies done in bovine Hsp70 homolog Hsc70. Lysine 71 of the Hsc70 is mutated into alanine, methionine and glutamic acid. All three of them had the same result, in which the hydrolysis activity was lost. Moreover, ATP binding cannot change the conformation of the protein in K71 mutants, thus peptide release does not occur in these mutations. K70 to alanine mutation in DnaK gives the same result [11].

T13 in Hsc70 is mutated into serine, valine and glycine to see the effect of T13 on the conformational changes triggered by ATP binding. ATP binding only changed conformation in the T13S mutant. These studies showed that the protein needs a hydroxyl group at that residue, which is why only T13S mutant had a conformational change [12].

In another study involving bovine Hsp70 homolog Hsc70, D10, D199, D206 and E175 are mutated into serine and asparagine for aspartic acid residues D10, D199, D206 and glutamine for E175 to find the residues that might participate in the ATP hydrolysis reaction. Mutations of the D10 and D199 reduce k_{cat} values to around 1% of the wild type, whereas D199 and E175 mutations reduce it around 10% of the wild type. Changes in K_m values are little in D199 and D206 mutants but increased 10-100 fold in the mutations of the D10 and E175. Those mutations are also visualized in crystal structures with ADP + Pi and AMPPNP (5′-adenylyl-β,γ-imidodiphosphate, a non-hydrolyzeable molecule which can take place of the ATP) bound models. Results of these experiments show that the ATP hydrolysis reaction

does not depend on just a single catalytic residue and the orientation of the Mg^{2+} ion is crucial for the reaction [13].

P143, R151 and E171 were mutated (glycine for P143, lysine for R151, aspartic acid for E171 and alanine for the all three of them) to observe their effects on the conformational changes between the ATP state and the ADP state. Results show that the mutations of P143 and E171 create a nonfunctional protein. Concerning the mutations of R151, alanine mutation cancels the allosteric control mechanism between the two domains. Lysine mutation abolished the DnaJ + substrate stimulation and reduced the substrate release rate to 6% of the wild type in the presence of ATP. With these results, an allosteric control mechanism involving E171 and K70 as sensors for ATP was proposed. These residues were suggested to affect the conformation of P143 so it can act as a switch and affect the position of R151. The latter then interacts with DnaJ and substrate and all of the conformational changes of these residues reverse in favor of an ideal conformation to catalyze ATP hydrolysis [14].

1.4 General Mechanisms For Phosphate Hydrolysis

Phosphate hydrolysis is an essential reaction for biological systems as they get the necessary energy to sustain their functions as a living organism from hydrolyzing ATP or GTP. Even though this reaction has great importance for life itself, the actual mechanism surrounding the phosphate hydrolysis is still unclear. However, there are two suggested reaction pathways. One of the two pathways is an associative pathway and the other one is a dissociative pathway.

What defines the reaction pathway as associative or dissociative is the distance between the γ-phosphate and the attacking nucleophile and the distance between the γ-phosphate to the leaving group at the transition state. This definition is applicable to the More O'Ferrall-Jencks diagrams [15].

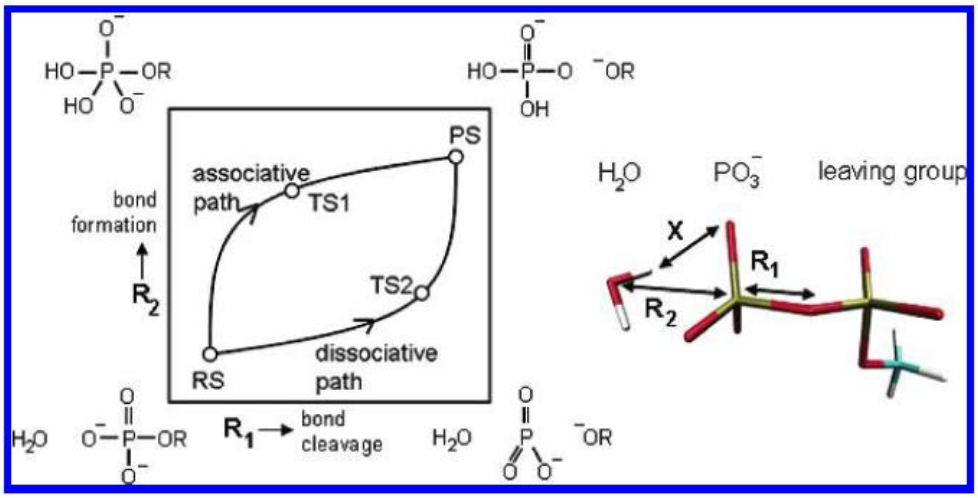

Figure 1.8 : A schematic description of the potential surface for the hydrolysis of phosphomonoesters with three reaction coordinates *R*1, *R*2 and *X* [15].

In the associative mechanism, the cleavage of the leaving group and the γ-phosphate is not advanced while a partial bond formation with the nucleophile occurs. The transition state is shaped as pentacovalent trigonal bipyramidal phosphorus. On the other hand, dissociative mechanism involves the dissociation of the leaving group before the nucleophile attacks. In this configuration, the transition state proceeds by metaphosphate formation. Proton transfer occurs after the dissociation in this pathway. Usually in an associative mechanism, the reaction begins with a proton transfer from the nucleophilic water to the γ-phosphate. Since γ-phosphate acts as a base, this type of associative mechanism is called the substrate assisted catalysis or substrate as a base mechanism. Both of the associative and the dissociative reaction pathways can either proceed as stepwise or concerted. Stepwise process involves proceeding through stable intermediates, whereas a concerted pathway proceeds through a single transition state. This transition state involves the bond formation with the nucleophile and the bond cleavage with the leaving group in one step.

There are several experimental studies (linear free energy relationships-LFER, measurement of activation entropy, kinetic isotope effect) to determine the pathway of the phosphate hydrolysis reaction. Most of the experiments are consistent with a dissociative mechanism. However, a study involving computationnal methods pointed out that the same experiments may also consistent with an associative mechanism under certain conditions. In another study, the same group which did the previous study obtained very similar activation energies for associative and

dissociative pathways. Based on this observation, they suggested that the architecture of different active sites may catalyze one mechanism or the other [16-24].

1.5 Suggested Mechanisms

With collective mutation and crystallography studies, it is suggested that there is not a single catalytic residue in the active site, but several amino acids work together to extract a H^+ or stabilize the nucleophilic OH^- ion. Given that their studies show that the mutation of the residues interacting with the coordination shell of the Mg^{+2} ion has a greater effect than the more distant residues, they thought that the Mg^{2+} ion has an important role in the reaction. Moreover, a H_2O molecule which has a positon to attack ATP cannot be seen in the crystal. Based on these results, they proposed a pathway which requires some rearrangements in the electrostatic interactions in each step. First, γ-phosphate of the ATP reorients itself to take a position such that a nearby water molecule can do an inline attack. With this reorientation, ATP forms a β,γ-bidentate complex with Mg^{2+}, which was interacting only with the b phosphate before. After this reorientation, attack by an OH^- ion or a watter molecule, which is the one interacting with K71, occurs. Final step involves the release of the Pi group. This suggestion relies heavily on the Mg^{+2} ion to position the γ-phosphate to initiate the hydrolysis reaction [3, 13].

Another mechanism is suggested from the computational studies using QM/MM reactive Car-Parrinello simulations in a study done with the T13G mutant of Hsc70, which is a mutation they think that provides high flexibility. As a result, triphosphate chain can be displaced easily. This also results with one of K^+ to get O atoms of γ-phosphate to its coordination shell. Empty space formed by this configuration is filled with the catalytic water molecule. This water molecule is in the coordination shell of the Mg^{2+} ion. Reaction starts with the dissociation of the catalytic water molecule into H^+ and OH^-. H^+ then attaches itself to the nearby O atom of the γ-phosphate. The OH^- ion remains in the coordination shell of the Mg^{2+} while the bond between P of the γ-phosphate and O of the β-phosphate is cleaved. HPO_3 becomes a leaving group and distances itself from ADP. The OH^- ion attacks after this step and forms $H_2PO_4^-$. The K^+ ion follows the leaving group starting with the step that involves the bond cleavage between β- and γ- phosphate. This ion is responsible for getting the OH^- ion to attack. Basically this mechanism suggests a reaction that is

caused by dissociation of a water molecule between the Mg^{2+} and the K^{+} ions. Reaction results in the formation of Pi and the shift of the attacking water molecule into the coordination shell of the K^{+} ion from Mg^{2+}. This suggestion completely ignores the possible roles of the residues in the active site and proposes the idea of HPO_3 to be a leaving group [25].

1.6 Aim of the Study

This study focuses on the ATP hydrolysis mechanism of the chaperone protein Hsp70. In particular, the roles of the critical residues and effects of the ions in the active site and the hydrolysis reaction type (associative or dissociative) were investigated.

Mutation studies show that K70, E171, D194, D201 and T199 may have catalytic activites and are very important in the ATP hydrolysis reaction. Especially some mutations of the K70, E171 and D194 create a nonfunctional protein. These residues and their possible roles were investigated in this study. Particular attention has been paid to the role of K70 as it is known experimentally that this residue is crucial for ATP hydrolysis. Geometry optimizations have been carried out on structures where this residue is coordinated to the nucleophilic water or oriented away from this water.

Moreover, this study assumes there can be an acid-base catalysis. Protonation states of the D194, D201 and E171 in the reactant and product structures were studied. The effect of these protonation states on the transition pathway was investigated.

It was shown in the literature that the active site needs Mg^{2+} and K^{+} ions to function properly. Previous studies on this subject highly emphasizes the orientations and the roles of those ions in the active site, so this study will contribute to clarify the roles of these two ions.

Phosphate hydrolysis reactions can take place either through an associative or a dissociative mechanism depending on the environment. Therefore, both mechanisms are tested in order to identify lowest energy pathway.

This study will use computational methods to provide evidence for the roles of the residues and the ions in the active site while showing the possible mechanism for the ATP hydrolysis in the *E. Coli* Hsp70 homolog DnaK.

2. MATERIALS AND METHODS

All calculations were performed with ONIOM method [26-28] as implemented in Gaussian09 software [29]. MM calculation were performed using the Amber ff03 force field [30], QM calculations were performed at the M06-2X level of theory, using the 6-31+G** basis set for oxygen atoms and 6-31G** for all other atoms in the model system. The choice of the M06-2X level was done according to the previous unpublished studies on phosphate hydrolysis reactions where high level QM methods were compared with various DFT methods. That study revealed that the M06-2X functional gave the most accurate results for phosphate hydrolysis reactions. For all atoms in the system the basis set is chosen to provide a polarization function (as a d-orbital) to the heavy atoms and p functions to the hydrogen atoms, leading to a more flexible wave function.

Our first geometry optimizations were performed via mechanical embedding. However in some cases, it was observed that one of the hydrogen atoms of K70 amino group was donated to ATP. But electronic embedding optimizations located the proton on K70 even if the proton was put manually on ATP in the initial geometry. Therefore, all optimizations were performed using the electronic embedding approach.

With respect to molecular dinamics simulations and thermodynamic integration studies done before in our group, we decided to create two different initial models depending on the protonation state of D201 (referred as 201N for neutral D201 and 201I for ionized D201). We then selected a snapshot for each of these models from those simulations.

Our QM region consists of the two loops surrounding the ATP and the catalytically important residues K70, E171, D194, T199 and D201 (Figure 2.1). Total atoms in the environment is 9061 with 175 atoms in the QM region and 8886 atoms in the MM region. Both the total number of atoms and the number of QM region atoms are the same in 201N model and 201I model because there is a second K^+ atom in the 201I model. QM region and MM region are seperated with hydrogen link atoms.

ONIOM creates problems during the numeric update of the 2nd derivative matrix. As a result we could not achieve the full convergence for transition state optimizations. The convergence criteria limits of Gaussian 09 are listed below:

The maximum components of force must be smaller than 0.000450 cut-off value,

Below 0.000300 cut-off value for Root Mean Square of the forces,

The calculated displacement for the next step must be below the cut-off value 0.001800 for Maximum Displacement,

Smaller than 0.001200 tolerance limit for RMS Displacement (Root Mean Square of the displacement) for the next step.

The maximum RMS Force among all of our transition structures is 0.000538. Hence, although not fully converged, we believe that our results are of semi quantitative quality.

2.1 Density Functional Theory

Density functional theory is a quantum mechanical method [31-34]. In quantum mechanics, unlike classical mechanics, the position and the momentum of a particle cannot be known simultaneously without any uncertainty. Therefore the position of a particle is expressed as a probability function, Ψ^2. Ψ is known as the wavefunction and is obtained by solving the Schrödinger equation:

$$\hat{H}\,\Psi(x) = E\Psi(x) \qquad (2.1)$$

$\hat{H}$ is the Hamiltonian operator, and it provides the energy (E) and the wavefunction of the system.

$$\hat{H}_{elec} = -\frac{1}{2}\sum_{i=1}^{N}\nabla_i^2 - \sum_{i=1}^{N}\sum_{A=1}^{M}\frac{Z_A}{r_{iA}} + \sum_{i=1}^{N}\sum_{j>1}^{N}\frac{1}{r_{ij}} = T + V_{Ne} + V_{ee} \qquad (2.2)$$

In 2.2, the first term gives the kinetic energy of electrons, the second term gives the attraction between electrons and nuclei, and the third term gives the interelectronic repulsion. Z_A is the charge of any nucleus, N the number of electrons, M the number

of nuclei, r_{ij} distance between electrons i and j, and r_{iA} distance between electron i and nucleus A.

There are many acceptable solutions of the Schrödinger equations, identified by the quantum number *n*:

$$\hat{H}\,\Psi_n(x) = E\Psi_n(x) \qquad n=1,2,\ldots \tag{2.3}$$

The exact solution of the Schrödinger equation exists only for one-electron systems. For many-electron systems only approximate solutions can be obtained. The first step to obtain these approximate solutions is the separation of variables by expressing the many-electron wavefunction $\Psi(1,2,3..)$ as the product of one-electron wavefunctions $\chi_1(1)$, $\chi_2(2)$, $\chi_3(3)$..

Such a separation is possible only if the electrons are independent from each other, which is of course not true in real systems. Therefore, the error introduced by the independent electron approximation must be corrected later in the calculations.

On the other hand, according to Pauli Exclusion Principle, the wavefunction must be antisymmetric with respect to the exchange of the labels of any two electrons [31-34]. Hence, expressing Ψ as the product of one-electron wavefunctions would violate the Pauli Exclusion Principle. Instead, Ψ is expressed as a Slater determinant:

$$\Psi_{SD} = \frac{1}{\sqrt{N!}} \begin{vmatrix} \chi_1(x_1) & \chi_2(x_1) & \cdots & \chi_N(x_1) \\ \chi_1(x_2) & \chi_2(x_2) & & \chi_N(x_2) \\ \vdots & \vdots & & \vdots \\ \chi_1(x_N) & \chi_2(x_N) & \cdots & \chi_N(x_N) \end{vmatrix} \tag{2.4}$$

which is constructed from a set of N single-electron wave functions (N being the number of electrons in the molecule) in Hartree-Fock theory. Every $\chi_i(x_N)$ function is equal to the spin function multiplied by the spatial wave function. The Schrödinger equation with a Hamiltonian in **(2.2)**, and Ψ given as a Slater determinant, can be reorganized as:

$$E_{HF} = \int \Psi_0 H_0 \Psi_0 \, d\tau = \sum_{i}^{N} (i \mid \hat{h} \mid i) + \tfrac{1}{2} \sum_{i}^{N} \sum_{j}^{N} (ii \mid jj) - (ij \mid ji) \tag{2.5}$$

$$(i \mid \hat{h} \mid i) = \int \chi_i^* (x_1) \left(-1/2 \, \nabla_i^2 - \sum_{A}^{M} Z_A / r_{iA}\right) \chi_i (x_1) \, dx_1 \tag{2.6}$$

$$(ii \mid jj) = \iint |\chi_i (x_1)|^2 1/r_{12} \, |\chi_j (x_2)|^2 dx_1 \, dx_2 \tag{2.7}$$

$$(ij \mid ji) = \iint \chi_i (x_1) \, \chi_j^* (x_1) \, 1/r_{12} \, \chi_j (x_2) \, \chi_j^* (x_2) \, dx_1 \, dx_2 \tag{2.8}$$

(2.6) gives the kinetic energy of a given electron and the interaction energy between this electron and the nuclei. The integral in (2.7) is known as the Coulomb integral (J), and gives the total Coulombic repulsion between any two electrons. The integral in (2.8) is called the exchange integral (K). It has no classical counterpart, and arises completely from the Pauli Exclusion Principle [31-34].

Each one-electron orbital (χ_i) can be approximated by using a linear combination of Gaussian functions, known as the basis set.

$$\chi_i = \sum_{\mu=1}^{N} c_{\mu i} \, \varphi_\mu \tag{2.9}$$

The energy calculated with a wave function, which is described with a basis set, is always higher than the exact energy. Therefore $c_{\mu i}$ values (molecular orbital expansion coefficients) are calculated by minimizing the energy, with respect to these coefficients. This procedure is called as variation principle.

The method described above is known as the Hartree-Fock method. Since this method starts with the independent electron approximation and the errors introduced by this approximation are never corrected, it lacks the electron correlation effects. This means that each electron moves in the average field created by all other electrons, without knowing their instantaneous positions. Therefore electrons can get unrealistically close to each other. There are methods which are based on the calculation of the wavefunction, and which can include the electron correlation effects, but these methods are computationally very expensive. Instead density functional methods offer a cheaper solution of this problem.

DFT is based on Kohn-Hohenberg theorems, which state that the electron density $\rho(r)$ includes all the information carried in Ψ. $\rho(r)$, which can be obtained from a many-electron wavefunction Ψ, is given by:

$$\rho(r_1) = N \int \ldots \int dr_2 \ldots dr_N \mid \Psi(r_1, r_2, \ldots r_N) \mid^2 \quad (2.10)$$

where r denotes both spin and spatial coordinates of electrons.

The first Kohn-Hohenberg theorem (Existence theorem) states that the electron density $\rho(r)$ determines the external potential v(r), i.e. the potential due to the nuclei. This means that for a given electron density, there exists only one particular distribution of nuclei with their given charges.

The second theorem introduces the variation principle, i.e. the energy computed with an approximate density is always greater than the true energy. Therefore the energy is minimized with respect to ρ(r).

Three variables in the energy, E(N, R_A, Z_A), can be known when electron density is known. The energy can be written as:

$$E[\rho] = \int v(r)\, \rho(r)\, dr + T[\rho] + V_{ee}[\rho] \quad (2.11)$$

where T[ρ] is the kinetic energy of the interacting electrons and $V_{ee}[\rho]$ is the electron-electron repulsion energy. Calculation of the kinetic energy of the interacting electrons is difficult. Therefore Kohn and Sham defined a reference system with non-interacting electrons, such that the one-electron wavefunctions of these electrons give the true density [30-33]. The wavefunction of this system can be expressed as a Slater determinant of one-electron functions χ_i(r) and the density can be written as;

$$\rho(r) = \sum_{i=1}^{N} |\chi_i(r)^2| \quad (2.12)$$

The kinetic energy of this system can be calculated by using χ_i(r)'s as in the Hartree-Fock theory. Now the electronic energy may be rewritten as:

$$E[\rho] = \int v(r)\, \rho(r)\, dr + T_{ni}[\rho] + J[\rho] + E_{xc}[\rho] \quad (2.13)$$

with $J[\rho]$ being the coulomb energy, $T_{ni}[\rho]$ being the kinetic energy of the non-interacting electrons and $E_{xc}[\rho]$ being the exchange-correlation energy functional. The exchange-correlation functional is an unknown functional and expressed as the sum of an exchange functional $E_x[\rho]$ and a correlation functional $E_c[\rho]$, although it contains a correctional term, which accounts for the kinetic energy term arising from the kinetic energy difference between the interacting and non-interacting electron systems.

Minimization of the energy with respect to $\rho(r)$, with the constrain that the one-electron orbitals are orthonormal, yields:

$$[\ (-1/2)\ \nabla_{KS}^{2} + V_{eff}(r)\ ]\ \chi_j(\mathrm{r}) = \varepsilon_i \chi_j(\mathrm{r}) \tag{2.14}$$

where ε_i is the orbital energy of the corresponding independent (χ_j) Kohn–Sham orbital.

In (2.14), the one-body potential V_{eff} can be defined as;

$$V_{eff} = v(\mathrm{r}) + [\ \partial J(\rho) / \partial \rho(r)\ ] + [\ \partial E_{xc}(\rho) / \partial \rho(r)\ ] \tag{2.15}$$

$$V_{eff} = v(\mathrm{r}) + [\ \rho(r') / |\ \mathrm{r}-\mathrm{r}'|\ ]\ \mathrm{d}r' + v_{xc}(r) \tag{2.16}$$

where $v_{xc}(r)$is the exchange-correlation potential.

The exact form of the exchange-correlation functional is not known. It is possible only for simple systems to derive these functionals. Therefore approximate forms are studied and improved. If we assume that the density is kept same everywhere, ρ=N/V, we can make our first approximation, i. e. the local density approximation (LDA). This approximation gives the energy of a uniform electron gas, i. e. a large number of electrons uniformly spread out in a cube accompanied with a uniform distribution of the positive charge to make the system neutral. The total energy of the system is expressed as a functional of the charge density as:

$$\mathrm{E}[\rho] = T_s[\rho] + \int \rho(r) v_{\mathrm{ext}}(r)\mathrm{d}r + J[\rho] + E_{xc}[\rho] + E_b \tag{2.17}$$

1. T_s is the Kohn–Sham kinetic energy functional, which is expressed in terms of the Kohn–Sham orbitals as:

$$T_s[\rho] = \sum_{i=1}^{N} \int\ \chi_i^*(r) \left[\left(-\frac{1}{2}\right)\nabla^2\right] \chi_i(r)\,dr \tag{2.18}$$

2. v_{ext} is the external potential which acts on the interacting system at minimum,
3. E_{xc} is the exchange-correlation energy,
4. E_b is the electrostatic energy of the positive background and since the positive charge density is the negative of the electron density due to uniform distribution of particles, the energy expression is reduced to:

$$\mathrm{E}[\rho] = T_{\mathrm{S}}[\rho] + E_{\mathrm{XC}}[\rho] \tag{2.19}$$

$$\mathrm{E}[\rho] = T_{\mathrm{S}}[\rho] + E_{\mathrm{X}}[\rho] + E_{\mathrm{C}}[\rho] \tag{2.20}$$

The kinetic energy functional T_s can be rewritten as:

$$T_S[\rho] = C_F \int \rho(r)^{5/3} dr \tag{2.21}$$

where C_F is a constant equal to 2.8712. The exchange energy functional can be calculated exactly by:

$$E_X[\rho] = -C_X \int \rho(r)^{4/3} dr \tag{2.22}$$

with C_x being a constant equal to 0.7386. Even for this simplest system, it is not possible to derive a similar approximation for the correlation energy, $E_c[\rho]$. Using Quantum Monte Carlo techniques, Ceperley and Alder (1980) calculated the total energy for uniform electron gases of several different densities to very high numerical accuracy. For each case, they were able to determine the correlation energy in these systems and the kinetic energy functional is obtained by fitting an analytical function to their results.

A disadvantage of the LDA method is the underestimation of the exchange energy by about 10 percent and it does not have the correct asymptotic behavior. The exact asymptotic behavior of the exchange energy density of any finite many-electron system is given by:

$$\lim_{x \to \infty} U_X^{\sigma} = -1/r \tag{2.23}$$

where U_X is the Coulomb potential of the exchange charge and U_X is related to total exchange functional, $E_X[\rho]$ by;

$$E_X[\rho] = \tfrac{1}{2} \sum_{\sigma} \int \rho_\sigma U_x^{\sigma} dr \tag{2.24}$$

To correct this problem, exchange-correlation functionals are created to have a proper asymptotic limit by adding a gradient correction term.

The adiabatic connection formula connects the non-interacting Kohn-Sham reference system (λ=0) to the fully-interacting real system (λ=1) and is given by:

$$E_{xc} = \int_0^1 U_{xc}^{\lambda} \, d\lambda \tag{2.25}$$

where λ is the interelectronic coupling-strength parameter and U_{xc}^{λ} is the potential energy of exchange-correlation at intermediate coupling strength. The adiabatic connection formula can be approximated by;

$$E_{XC} = ½\ E_X^{exact} + ½\ U_{XC}^{LD} \quad (2.26)$$

The equation 2.26, which is known as adiabatic connection formula, is the sum of exact and approximated exchange-correlations. This provides an accurate theory of the exchange-correlation functional and is the starting point of many approximations. The functionals which include an exchange term, are called hybrid functionals.

The functional used in this thesis is M06-2X. It belongs to a family of functionals, including also M06 and M06-L, where the main difference being the amount of the exact exchange. It is designed by Zhao *et al.* [35] and is a hybrid meta-generalized gradient approximation. The reason why they are called hybrid functionals is the addition of Hartree-Fock exchange functional into pure DFT functionals. They are also called latest generation functionals and used extensively in recent years because of their accuracy, and this accuracy of calculation depends upon the exchange-correlation functional, $E_{xc}[\rho]$.

The pure DFT parts (meta-GGA) depend on spin density (ρ), reduced spin density gradient (x) and kinetic energy functional [$T(\rho)$]. The reduced spin density gradient (x_σ) is shown in (2.27):

$$x_\sigma = |\ \nabla\rho_\sigma\ |\ /\ \rho_\sigma^{4/3}\ (\sigma = \alpha, \beta) \quad (2.27)$$

The M06 functional family includes 3 additional terms; Z as a working variable, γ and h as working functions.

$$Z_\sigma = [2\tau_\sigma\ /\ \rho_\sigma^{5/3}]\ -\ C_F,\ C_F = 3/5\ (6\pi^2)^{2/3},\ \gamma(x_\sigma, Z_\sigma) = 1 + \alpha(x_\sigma^2 + Z_\sigma) \quad (2.28)$$

$$h(x_\sigma,Z_\sigma)=[d_0/\gamma(x, Z)]+[(d_1x_\sigma^2+d_2Z)/\ \gamma^2(x, Z)]+[(d_3x_\sigma^4+d_4x_\sigma^2Z_\sigma + d_5Z_\sigma^2)/\gamma^2(x, Z)] \quad (2.29)$$

The exchange functional term ($E_x[\rho]$) of the M06-2X functional is kept same as in the M06-L functional:

$$E_x^{M06} = \sum_\sigma \int [\ F_{x\sigma}^{PBE}(\rho_\sigma(r), \nabla\rho_\sigma(r))\ \ f(\omega_\sigma) + \varepsilon_x^{LDA} h_x(x_\sigma,z_\sigma)]\ dr \quad (2.30)$$

where $h_x(x,z)$ is defined in (2.29). $F_x^{PBE}(\rho_\sigma(r), \nabla\rho_\sigma(r))$ indicates the exchange energy density, which is taken from PBE exchange model. According to Zhao *et al.*, PBE

model satisfies the correct uniform electron gas (UEG) limit and also gives rather good results in the non-covalent interactions [31].

$\varepsilon_{x\sigma}^{LDA}$ is the local spin density approximation for exchange;

$$\varepsilon_{x\sigma}^{LDA} = -3/2\ (3/4\pi)^{1/3}\rho_{\sigma}^{4/3}(r) \tag{2.31}$$

and the $f(\omega_\sigma)$ is the spin kinetic energy density factor;

$$f(\omega) = \sum_{i=0}^{m} a_i\, \omega_\sigma^{\,i} \tag{2.32}$$

where the variable $\omega_\sigma$is the function of t_σ, and the t_σ is the function of spin kinetic energy density (T) and spin density (ρ_σ).

$$\omega_\sigma = (t_\sigma - 1) / (t_\sigma + 1) \tag{2.33}$$

$$t_\sigma = T_\sigma^{LDA} / T_\sigma \tag{2.34}$$

where

$$T_\sigma^{LDA} \equiv 3/10\ (6\pi^2)^{2/3}\rho_\sigma^{5/3} \tag{2.35}$$

The correlation functional form of the M06-2X functional is again kept same as in their M06-L functional family. However, in this new correlation functional, the opposite spin and parallel spin correlations are treated differently by Truhlar and co-workers.

The opposite spin M06 correlation energy is given by;

$$E_C^{\alpha\beta} = \int e_{\alpha\beta}^{UEG}\ [\, g_{\alpha\beta}(x_\alpha, x_\beta) + h_{\alpha\beta}(x_{\alpha\beta}, z_{\alpha\beta})]\ dr \tag{2.36}$$

where $g_{\alpha\beta}(x_\alpha, x_\beta)$ is described as:

$$g_{\alpha\beta}(x_\alpha, x_\beta) = \sum_{i=0}^{N} C_{C\alpha\beta,i}\ [\gamma_{C\alpha\beta}\,(x_\alpha^{\,2} + x_\beta^{\,2}) / 1 + \gamma_{C\alpha\beta}\,(x_\alpha^{\,2} + x_\beta^{\,2})\,]^{\,i} \tag{2.37}$$

and $h_{\alpha\beta}(x_{\alpha\beta}, z_{\alpha\beta})$ is described in (2.29) with $x_{\alpha\beta}^{\,2} \equiv x_\alpha^{\,2} + x_\beta^{\,2}$ and $z_{\alpha\beta} \equiv z_\alpha + z_\beta$.

The parallel spin correlation energy is;

$$E_C^{\alpha\alpha} = \int e_{\alpha\alpha}^{UEG}\ [\, g_{\alpha\alpha}(x_\alpha) + h_{\alpha\alpha}(x_\alpha, z_\alpha)]\ D_\alpha\, dr \tag{2.38}$$

where this time $g_{\alpha\alpha}(x_\alpha)$ is described with:

$$g_{\alpha\beta}(x_\alpha, x_\beta) = \sum_{i=0}^{N} C_{C\alpha\alpha,i} \; [\, \gamma_{C\alpha\alpha} (x_\alpha^2) \,/\, 1+ \gamma_{C\alpha\alpha} (x_\alpha^2) \,]^{\,i} \qquad (2.39)$$

In (2.38), D_α is the self-interaction correction term for avoiding self-interactions:

$$D_\alpha = 1 - (\, x_\alpha^2 \,/\, 4 \, [\, z_\alpha + C_F] \,) \qquad (2.40)$$

If the system is a one-electron system, Equation 2.39 will be meaningless. The terms $e_{\alpha\beta}^{UEG}$ and $e_{\alpha\alpha}^{UEG}$ are the uniform electron gas correlation energy density for opposite spinned and parallel spinned systems.

The total M06 correlation energy can be written as the sum of opposite spinned and parallel spinned components:

$$E_C = E_C^{\alpha\beta} + E_C^{\alpha\alpha} + E_C^{\beta\beta} \qquad (2.41)$$

The $\gamma_{C\alpha\beta}$ and $\gamma_{C\alpha\alpha}$ terms in the (2.37) and (2.39) are constants equal to 0.0031 and 0.06, respectively [34].

All of energies form the hybrid meta-generalized functional. The hybrid exchange-correlation energy ($E_{XC}[\rho]$) now can be written as;

$$E_{XC} = (X/100) \, E_X^{HF} + [1-(X/100)] \, E_X^{DFT} + E_C^{DFT} \qquad (2.42)$$

Where E_X^{HF} is the nonlocal Hartree-Fock exchange energy and X is the percentage of this Hartree-Fock exchange energy in the hybrid functional. The X value is optimized to obtain the best results. In addition to X value, all the parameters in the equations are optimized against accurate data too [37].

For observing the accuracy of the M06-2X method, some comparisons were done. These comparisons consisted of hybrid functionals, pure DFT functionals and functionals with full Hartree-Fock exchange. According to Zhao *et al*., it performed better than all other functionals for calculation of the atomization energies, ionization potentials, electron affinities and proton affinities [35]. The M06-2X method also performed better to calculate the alkyl-bond dissociation energies, proton affinities of conjugated π systems, binding energies of a Lewis acid-base complex, heavy-atom transfer barrier heights [37, 40].

2.2 Basis Set

A basis set is a set of functions used to build the molecular orbitals. In the first quantum mechanical calculations using the Hartree-Fock theory, molecular orbitals (MO) were calculated with the Linear Combination of Atomic Orbitals (LCAO) technique, which is described in (2.9).

The approximation of molecular orbitals as the sum of one-electron atomic orbitals provided an easiness. These atomic orbitals are typically Slater-type orbitals (STO), defined by;

$$S_{nlm}(r,\theta,\varphi) = Nr^{n-1}e^{-\zeta}Y_l^m(\theta,\varphi) \tag{2.43}$$

where N is a normalization factor in the radial part, n is the principal quantum number of the orbital, ζ is called the orbital exponent (which controls the width of the orbital) and Y_l^m is the spherical harmonic. These orbitals can also be written with the Cartesian coordinates:

$$S_{abc}(x, y, z) = Nx^a y^b z^c e^{-\zeta r} \tag{2.44}$$

One can see that these functions depend on quantum numbers (n,l,m) and decrease exponentially with distance from the nuclei. The difficulty of the integration process of this type of orbitals, led to some approximations. If the exponential term is written as $\exp(-\zeta r^2)$, thefunction becomes a Gaussian type function (GTO):

$$Nx^a y^b z^c \exp(-\zeta r^2) \tag{2.45}$$

which is called a primitive, an individual Gaussian function. With Gaussian functions the electron integrals can be solved analytically. Except that the Gaussian functions decay faster than Slater-type functions at large r values, this approach was better than STO's, yet it was still taking longer to solve these integrals. To cure this problem, Pople and his co-workers proposed the minimal basis sets. They determined optimal contraction coefficients and exponents for mimicking STOs with contracted GTOs for a large number of atoms.

With this approximation, a linear combination of Gaussian functions is treated as a single function. This linear combination of primitive Gaussian functions is called a contracted Gaussian function. Therefore this type of basis sets are called STO-nG basis sets, where n is the number of primitive Gaussian orbitals mimicking a single

STO, varying from 2 to 6 **(2.45)**. Higher the number of these primitive Gaussian functions better is the accuracy.

$$S_{abc}(x, y, z) = N \sum_{i=1}^{n} c_i x^a y^b z^c \exp(-\zeta r^2) \quad (2.46)$$

This summation of linear combinations of Gaussian functions made the computation much easier, but the minimality was the problem. As one can see, there is only one contracted basis function defined for each type of orbital, either core or valence. A split-valence basis uses only one contracted basis function for each core atomic orbital, and multiple basis functions for the valence atomic orbitals. Therefore these types of basis sets are called split-valence basis sets. The simplest split-valence basis sets are called Pople basis sets, which are created by Pople and co-workers, and they used the *X*-*YZ*G notation. *X* is the number of primitives for the core orbitals, but *Y* and *Z* indicate that the valence orbitals are composed of two contracted basis functions, the first one is composed of a linear combination of *Y* primitive Gaussian functions, the other one is composed of a linear combination of *Z* primitive Gaussian functions.

Basis sets can be modified with two functions, which are polarization functions and diffuse functions. The first one, polarization functions add higher angular momentum orbitals for any heavy atom in the system. This addition permits polarization of the wave function and gives flexibility to electrons.

The second function is the diffuse function, which is useful for systems which have anions, weak interactions, lone pairs. The diffuse function permits the orbitals to occupy larger spaces. Basis sets with diffuse function are important for systems where electrons are relatively far away from the nucleus, as systems with significant negative charge and so on.

The selection of a basis set for quantum chemical calculations is very important and calculations can often be improved by the addition of diffuse and polarization functions [36, 39].

2.3 ONIOM

Hybrid methods are methods which combine two or more computational techniques in one calculation and allow analyzing the chemistry of very large systems with high precision. Most hybrid methods combine a quantum mechanical QM method with a MM method, which is generally referred to as QM/MM methods. The other class of hybrid methods combines (QM) method with (QM) method. The ONIOM (**O**ur own **N**-layered **I**ntegrated molecular **O**rbital and molecular **M**echanics) scheme can combine any number of molecular orbital methods as well as molecular mechanics methods. The region of the system where the chemical process takes place, as bond breaking or bond formation, is treated with an appropriately accurate method, while the rest of the system is treated at a lower level. QM/MM schemes provide opportunity to investigate enzyme reactions by treating the active site via a high level method, such as DFT, and the protein environment with less expensive method, by molecular mechanics.

Hybrid methods have some more differences, not only the different methods they combine but the treatment of covalent interaction between the QM and MM region (high and low level region) could change according to the method used. During the QM calculations dangling bonds are formed which must be saturated. Simplest approach to solve this problem is to use link atoms (LAs). Link atoms could be any atom that mimics the part of the system it substitutes but usually hydrogen atoms are used. Link atoms are used in a large proportion of QM/MM implementations as well as ONIOM scheme.

The second main difference between various QM/MM methods is the way the electrostatic interaction between the two layers is managed. Two different approaches are used to evaluate the electrostatic interaction. In *classical* or *mechanical embedding* approach the electrostatic interaction is evaluated as the interaction of the MM partial charges with partial (point) charges assigned to the atoms in the QM region.

In the second approach referred to as *electronic embedding*, the charge distribution of the MM region interacts with the wave function of the QM region. As a result electrostatic interaction are more accurately described in *electronic embedding* since the partial charges from the MM region are included in the QM Hamiltonian, by

allowing the wave function to respond to the charge distribution of the MM layer [26-28, 40].

The ONIOM energy expression is written as an extrapolation, in contrast to the merged Hamiltonian of traditional QM/MM methods. The ONIOM method works by approximating the energy of the whole system as a combination of the energies computed by less computationally expensive means:

$$E^{ONIOM} = E^{low}(Real) + E^{high}(Model) - E^{low}(Model) \quad (2.47)$$

In ONIOM, the real system contains all the atoms and is calculated only at the MM level. The model system contains the part of the system which is treated at the QM level with the link atoms that are used to cap dangling bonds resulting from cutting covalent bonds between the QM and the MM regions. Both QM and MM calculations need to be performed for the model system (see Figure 2.3. for the definition of the real and model systems and link atoms).

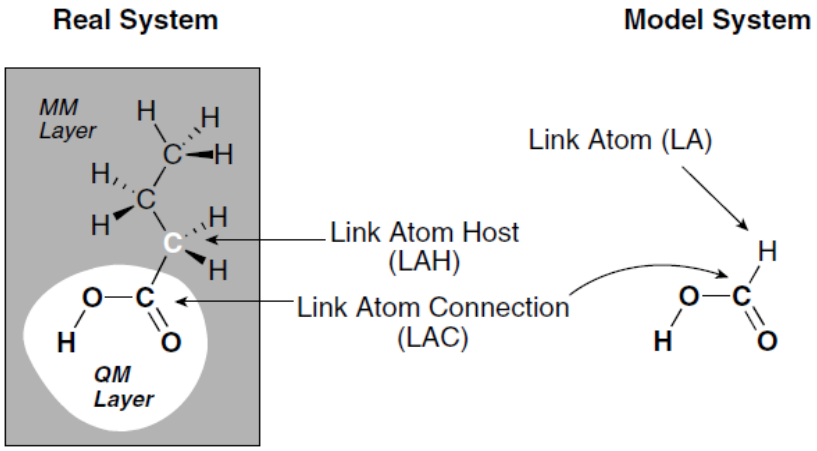

Figure 2.1 : The components of the ONIOM scheme [28].

2.4 MM Force Fields

Force fields can be described by parameters for all of the bonds, angles, dihedrals, and atom types in the system. In the context of molecular modeling, a force field refers to a collection of equations and related constants designed to reproduce molecular geometry and to describe the potential energy of a system.

Force field functions and parameter sets are derived from both experimental work and high-level quantum mechanical calculations. A force field is composed of

bonded terms and non-bonded terms. Bond stretching, angle bending and torsion angle represent bonded terms, while, van der Waals and Coulomb forces are classified into non-bonded terms contributions (Figure 2.4).

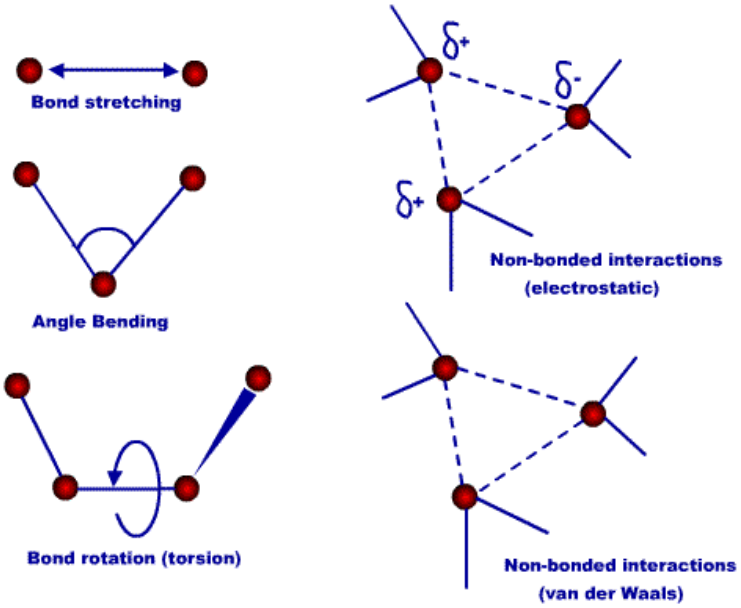

Figure 2.2 : Force field elements.

A general form for the total energy in an additive force field can be written as

$$E_{total} = E_{bonded} + E_{nonbonded} \tag{2.48}$$

the components of the covalent and noncovalent contributions are given by the following summations:

$$E_{bonded} = E_{bond} + E_{angle} + E_{dihedral} \tag{2.49}$$

$$E_{nonbonded} = E_{van\ der\ Waals} + E_{electrostatic} \tag{2.50}$$

$$E_{total} = \sum_{bonds} \frac{1}{2} k_i^{bond} (r_i - r_0)^2 + \sum_{angles} \frac{1}{2} k_i^{angle} (\theta_i - \theta_0)^2$$

$$+\sum_{dihedrals} k_i^{dihe} \left[1 + \cos(n_i \phi_i + \delta_i)\right]$$

$$+\sum_i \sum_{j \neq i} \left[\left(\frac{\sigma_{ij}}{r_{ij}}\right)^{12} - \left(\frac{\sigma_{ij}}{r_{ij}}\right)^{6}\right] + \sum_i \sum_{j \neq i} \frac{q_i q_j}{\epsilon r_{ij}} \tag{2.51}$$

The functional form of the AMBER force field is the sum of the equations (2.49) and (2.50) shown as equation (2.51) above [30, 41, 42]. The force is the derivative of this potential with respect to position.

The bonded interactions, formed by all chemical bonds, angles, and dihedrals which are present in the system are described respectively by the first three terms of the equation shown above. First term represents the energy between covalently bonded atoms. This harmonic force is a good approximation near the equilibrium bond length, but becomes increasingly poor as atoms separate. The second term represents the energy due to the change of an angle between two consecutive covalent bonds. Third term represents the energy for twisting a bond due to bond order (e.g. double bonds) and neighboring bonds or lone pairs of electrons.

The fourth term of the equation describes the van der Waals interactions between each pair of atom in the system. The form of the van der Waals energy is calculated using the equilibrium distance (r_{0ij}) and well depth (ϵ).

The fifth term represents the electrostatic interactions between atom pairs and is evaluated using Coulomb's law. The partial charges on atoms q_i and q_j are parameters.

The non-bonded interactions are not calculated between two covalently bonded atoms or between the first and third atoms in a covalently bound sequence because these interactions are already accounted for in the bond stretching and angle bending terms. The 1-4 non-bonded interactions are calculated but scaled.

3. RESULTS AND DISCUSSION

Two main models based on the protonation state of the D201 have been prepared for investigation of the ATP hydrolysis mechanism in DnaK. Initial geometries of these two models are obtained from the snapshots of molecular dynamics simulations carried out in a previous study in our group. Derivatives of these models are produced by manually altering the resulting geometry. The model with a neutral D201 is named 201N and the model with an ionized D201 is named 201I for convenience. Similarly, the names of all stationary points in the reactions of 201N and 201I have the suffix **N** or **I**, respectively.

3.1 Hydrolysis in the 201N System

Several transitions structures and products have been optimized for the 201N system. Their energies relative to the most stable reactant structure are displayed in Table 3.1.

Table 3.1 : Relative energies (with respect to **RN**) of the stationary points in the reaction of 201N.

NAME	Relative energy (kcal/mol)
RMgN	20.4
PN	-6.2
TSN1	28
TSN2	56.6
TSN3	60.2
AcidWN	31.3

In the reactant structure of the 201N model (**RN**, Figure 3.1), D201 and T199 are oriented away from the active site. Mg^{2+} is coordinated by β-phosphate and 5 nearby

water molecules. K70 interacts with the γ-phosphate and a nearby water molecule hydrogen bonded to E171, but does not interact with the attacking water. E171 interacts with the protonated side chain of D194 and a water molecule in the solvation shell of K^+. A second K^+ ion, observed in the crystals, is not present because it always leaves the active site in the molecular dynamics simulations when D201 is neutral. D194 only interacts with a water molecule solvating the γ-phosphate.

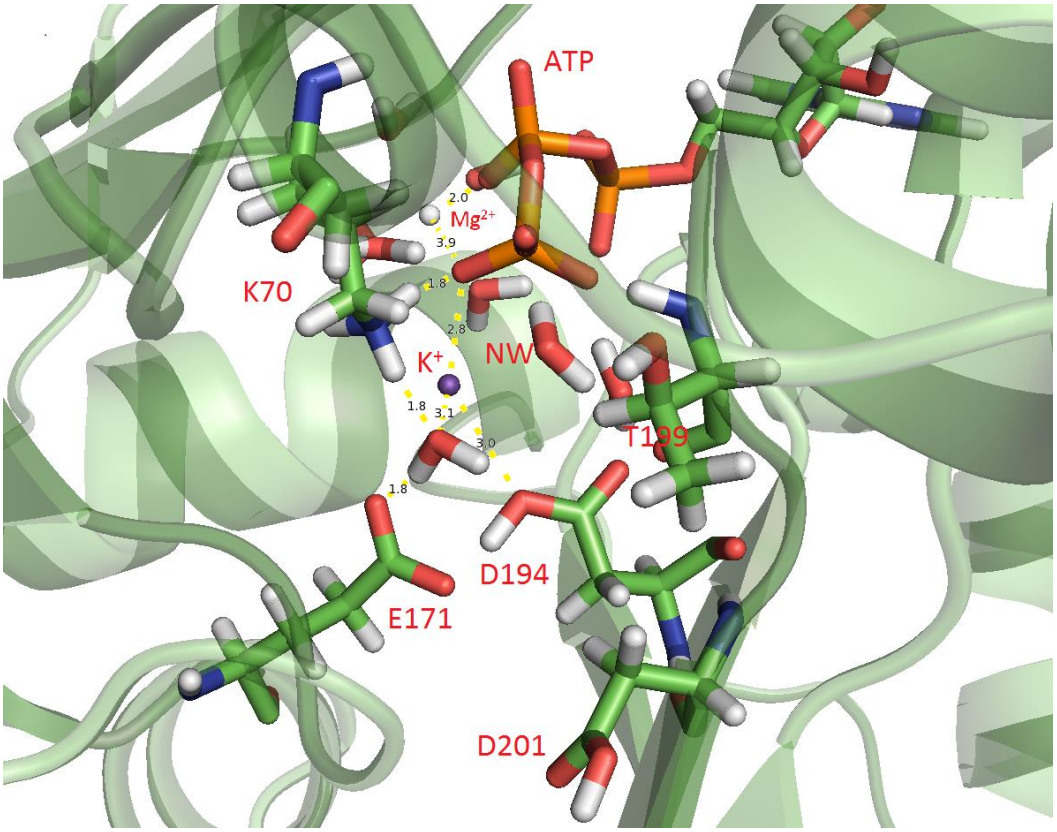

Figure 3.1 : The most stable reactant structure (**RN**) in the 201N system.

To test the hypothesis that Mg^{2+} can initiate the ATP hydrolysis as suggested in the literature, this ion has been placed between the β- and γ- phosphate groups and its coordination shell has been rearranged according to its new position [3]. Upon geometry optimization, configuration of the active site has remained the same as **RN**, except that the new position of the Mg^{2+} has caused K^+ to move 0.1 Å away from γ-phosphate (**RMgN**, Figure 3.2). The energy of this model is 20.4 kcal/mol relative to **RN** (Table 3.1). Considering that the shift in the position of Mg^{2+} is suggested to initiate the reaction, this type of reaction is not energetically feasible.

Several product structures differing in the position of Mg^{2+} or protonation states of Pi, E171 and D194 have been optimized. One of these structures corresponds to the product immediately formed after hydrolysis starting with **RN** where Mg^{2+} is coordinated only to β-phosphate (**PN**, Figure 3.3). On the other hand, since in the crystallographic structure Mg^{2+} is coordinated to both β- and γ-phosphates, the possibility of a shift in the position of this ion has also been investigated.

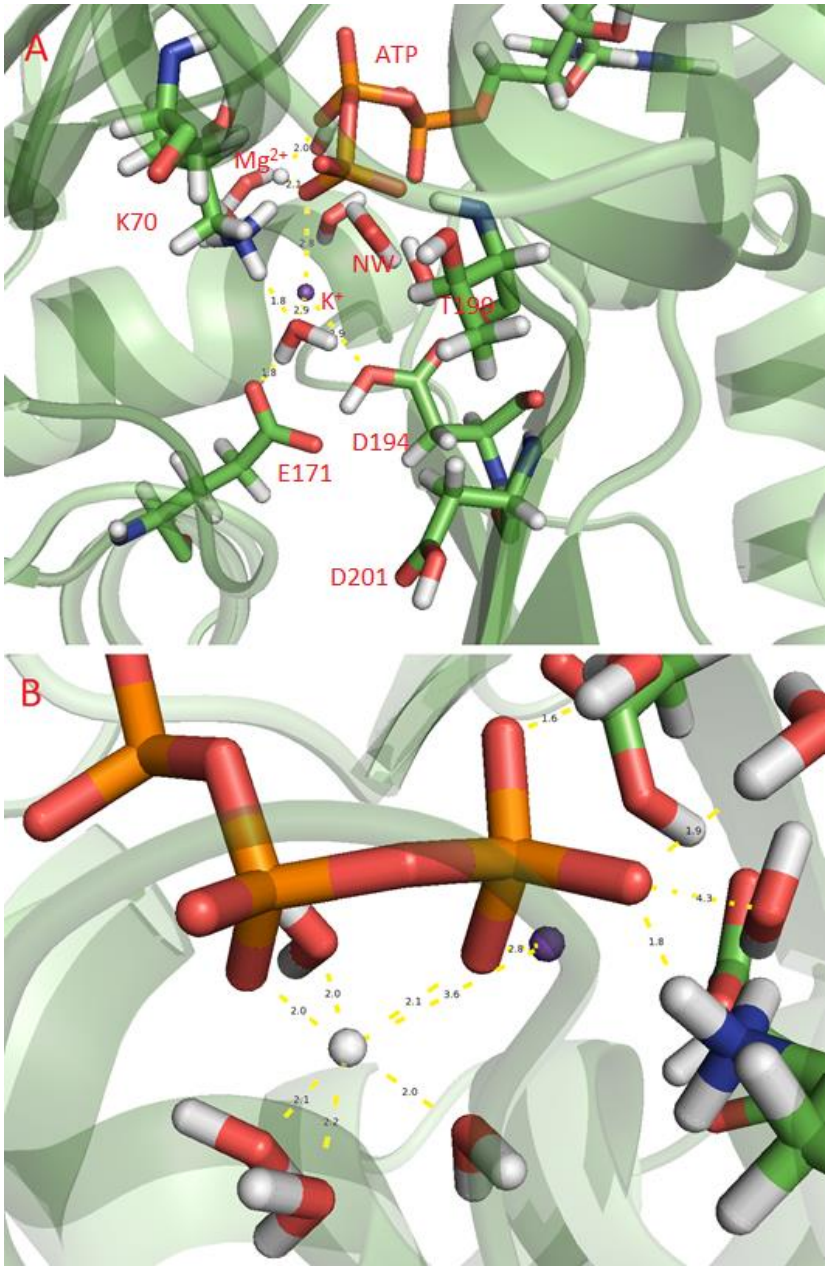

Figure 3.2 : Alternative reactant structure where Mg^{2+} is coordinated to both β- and γ-phosphates A) in the same orientation as Figure 3.1, B) close view of the coordination shell of Mg^{2+} in an orientation rotated by 90° with respect to (A).

In **PN** (the structure formed immediately after hydrolysis before any possible rearrangement of the Mg^{2+} position), positions of D194, E171, D201, T199 and K70 are almost the same as in **RN** (Figure 3.3). There are minor changes in the H-bond lengths and the K^+ ion is shifted as a result of the Pi formation, coordinating with the O atoms of E171 and D194 (0.2 Å towards E171 and D194, from 3.1 Å and 3.0 Å respectively, relative to the reference reactant structure). K70 interacts with an O atom of Pi. The relative energy of this product structure is -6.2 kcal/mol (Table 3.1). One of the protons of $H_2PO_4^-$ is oriented towards ADP, whereas the other proton interacts with a water molecule coordinated to D194.

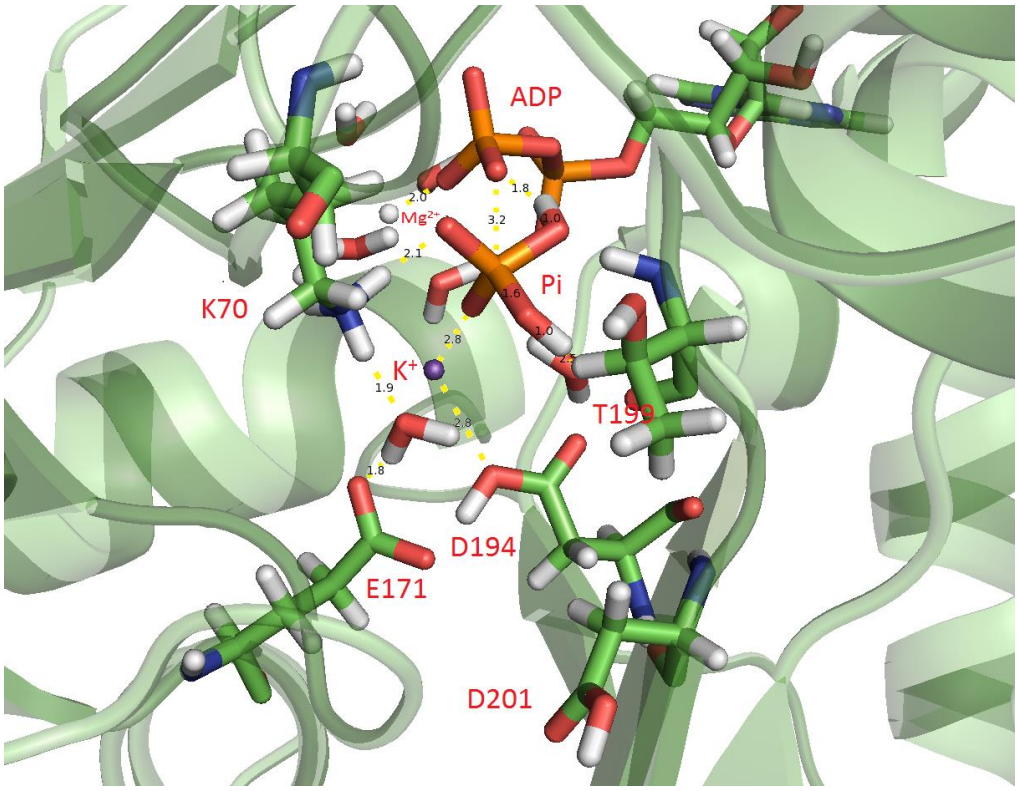

Figure 3.3 : The most stable product structure (**PN**) in the 201N system.

To test whether an arrangement like in the crystallographic ADP + Pi structure is more stable than **PN**, the Mg^{2+} ion has been positioned manually between β- and γ-phosphates and its coordination shell has been rearranged accordingly. Several attempts to optimize such a structure have always ended up with a shift of Mg^{2+} back to the β-phosphate as in **PN**.

A transition structure containing a four-membered ring has been optimized (**TSN1**). This transition state has an associative character with a cleaving bond length of 2.2A and forming bond length of 1.7 Å (Figure 3.4). The proton separated from the

nucleophilic water is already bonded with the γ-phosphate. Together with the long cleaving bond distance, this indicates a late associative transition state. Since the proton acceptor is ATP, this transition state corresponds to a substrate assisted catalysis mechanism. In this structure, K70 does not interact directly with the nucleophilic water. The oxygen of OH^- is solvated by a water molecule that also solvates D194. The H of OH^- makes a H-bond with another water molecule (1.8 Å). This interaction is not present in the **RN**. The same water molecule interacts also with K70. This interaction distance increases in going from the reactant to the transition state. K^+ also shifts by 0.1A towards a nearby O of the γ-phosphate.

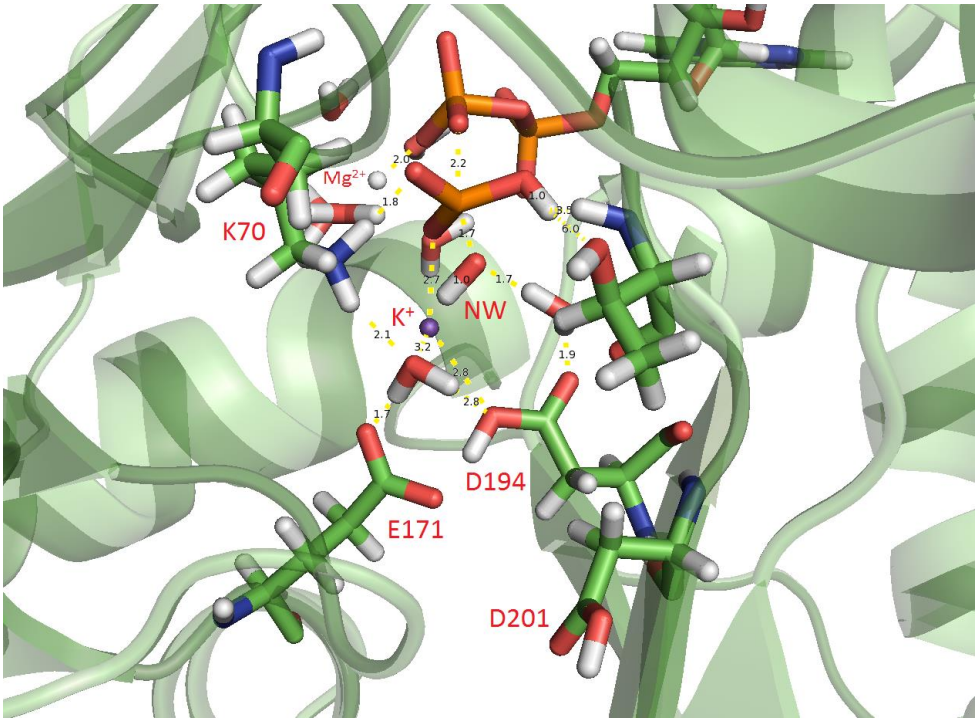

Figure 3.4 : The associative transition state (**TSN1**) without the assistance of K70 or T199.

The relative energy of this structure is 28kcal/mol (Table 3.1). This value is close to the activation enthalpy previously measured in the literature (26 kcal/mol) [14]. The computational methods used in our study are not accurate enough to interpret energy differences of 1-2 kcal/mol, nevertheless this result is remarkable. Since in **TSN1** there is no participation of K70 or T199, which are known to be catalytically important residues, its relative energy puts an upper limit to the activation energy for the substrate assisted mechanism. If those residues participate during the transition, one may find significantly lower relative energy. Orientation of T199 in 201N model

cannot do this type of interaction. Because of this, a model with both of these residues participating the reaction is considered in 201I model.

Alternative mechanisms involving acid-base catalysis have also been studied. Candidates for an acid role are a water molecule between Mg^{2+} and K^{+}, K70 and D194 whereas candidate for a base role is E171.

A second transition structure with E171 as a proton acceptor has been optimized (**TSN2**). This transition also has associative character with 2.3 Å for the cleaving bond and 1.8 Å for the forming bond (Figure 3.5). Proton transfer to E171 through a water molecule is completed. This transition state has a cleaving bond length 0.1 Å longer than **TSN1**, which suggests this geometry is also indicates a late associative transition state. In this structure, K70 interacts with both the leaving γ-phosphate group and nucleophilic water. OH^{-} is solvated by the same water as in **TSN1**. Relative energy for this structure is 56.6 kcal/mol. Even though K70 stabilizes OH^{-} unlike **TSN1**, this structure has much higher energy. This suggests that the E171 as a proton acceptor in the mechanism without a proton donor is not energetically favorable.

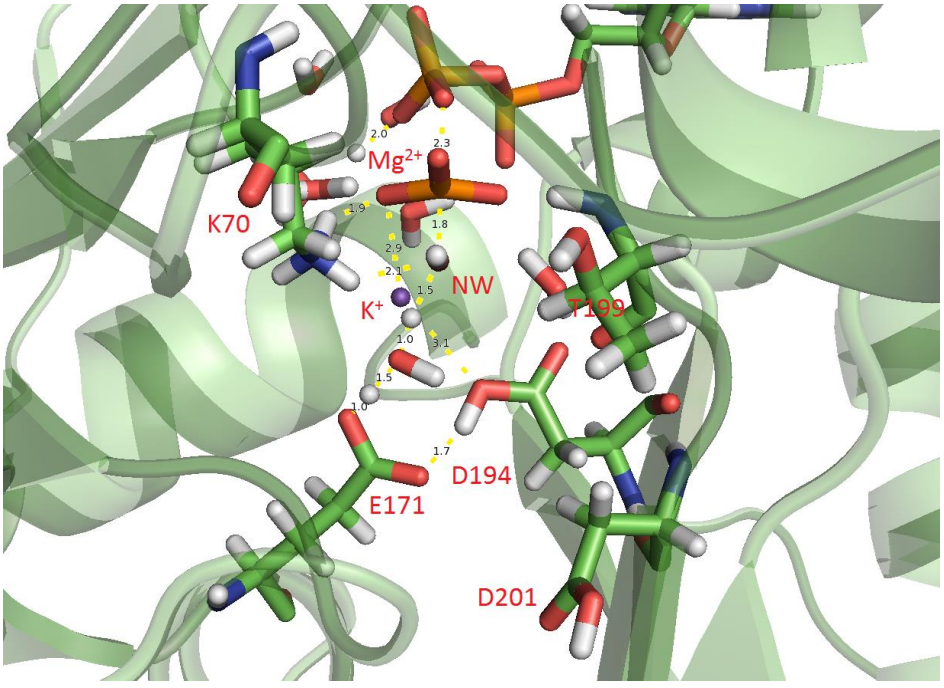

Figure 3.5 : The associative transition state (**TSN2**) without a proton donor.

Our third transition structure (**TSN3**) corresponds to acid-base catalysis with D194 as the proton donor and E171 as the proton acceptor (Figure 3.6). This transition state

has an associative character with a cleaving bond length of 1.9 Å and forming bond length of 2.1 Å. Proton from D194 is already bonded to the ATP. Proton transfer from the nucleophilic water to E171 occurs with the assistance of a second water molecule. Proton from this water is already accepted by E171 at the TS, but the proton transfer from nucleophilic water is not complete. K70 does not interact with the nucleophilic water directly; instead, it interacts with the leaving phosphate group and the water which passes its proton to E171. K^+ interacts with and stabilizes all of the nearby negative charges. Relative energy for this structure is 60.2 kcal/mol. This result shows us that an acid-base catalysis where D194 acts as an acid as the reaction mechanism is not energetically favorable. Before this optimization, we tried to optimize a structure with D194 donating a proton to ATP so that the active site environment can sort itself accordingly. Relative energy to the **RN** for that structure is 30 kcal/mol. The reason why there is a very high relative energy for the **TSN3** could be that the environment did not properly rearrange itself for this situation. But since giving a proton to the ATP requires energy, the result for **TSN3** will still be high for it to be energetically favorable. If this residue does not have a role in acid-base catalysis, the role of D194 could be positioning another residue or residues in the active site.

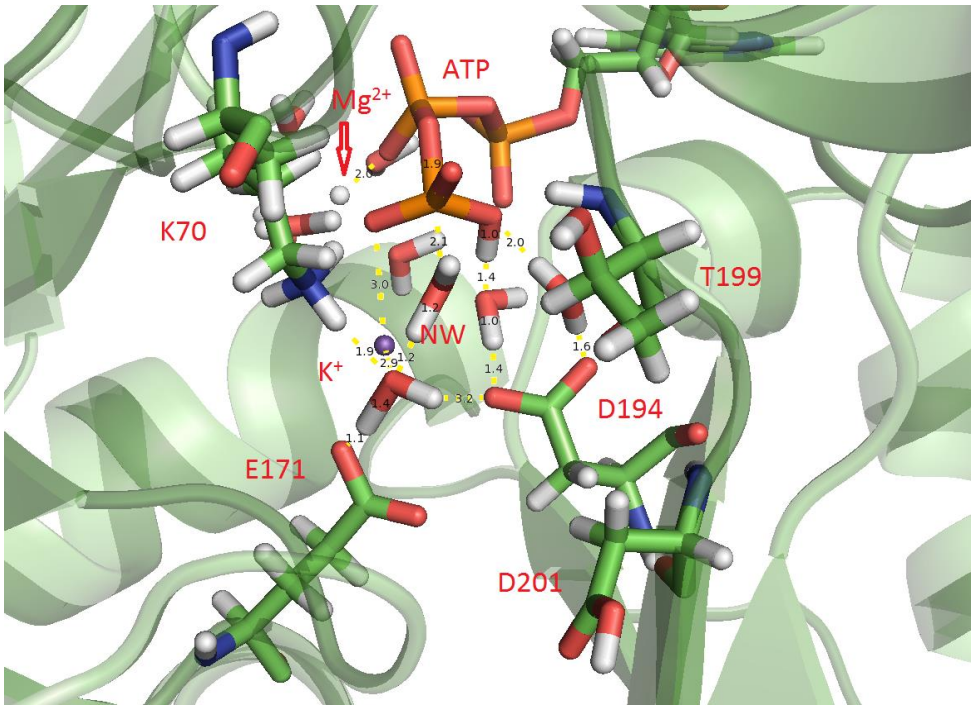

Figure 3.6 : Associative transition state (**TSN3**) with D194 as a proton donor and E171 as a proton acceptor.

A water molecule between Mg^{2+} and K^+ has been deprotonated to give a proton to γ-phosphate as an initiator for the reaction. Even though one may think that it is possible for this water molecule to be deprotonated as it has a low pKa because of its position between the two cations, the proton did not create a bond with the γ-phosphate and shifted back to its original position upon geometry optimization. Because of that, the optimization has been conducted with freezing the bond between the proton and the accepting O atom. Removing the constraint has still resulted in the same geometry as before, so to see the energy difference, whole optimization process has had to be conducted with freezing the bond. In the optimized geometry (**AcidWN**), K^+ shifted itself away from E171 and D194 to stabilize the OH^- ion better. K70 is also oriented away from γ-phosphate to interact with a nearby water molecule (Figure 3.7). Relative energy of this model is 31.3 kcal/mol, too high to be the initial step of a general acid catalyzed reaction. Nevertheless, we have attempted to optimize a transition state for the hydrolysis reaction following the proton transfer from this water molecule. The proton migrated back to water during optimization.

One of the mechanisms proposed in the literature also begins with such a proton transfer, followed by the attack of the OH- ion formed by this proton transfer [25]. Our results indicate that this pathway is unlikely.

K70 would be another candidate as an acid. But when we tried to do a geometry optimization with K70 giving one of its protons to ATP, it resulted in the shift of the proton to its original position. Nevertheless, we also attempted to optimize a TS, but the optimization collapsed back to the reactant structure.

With two of the optimizations collapsing back to the reactant structure and one with a very high relative energy suggests that acid-base catalysis is not likely to occur.

We tried to search for a dissociative transition state but those tests always resulted in going to the reactant or product states.

The relative energies of all of our 201N models can be seen in the energy versus reaction path graph (Figure 3.8.), where unlikely mechanisms are shown in dashed lines.

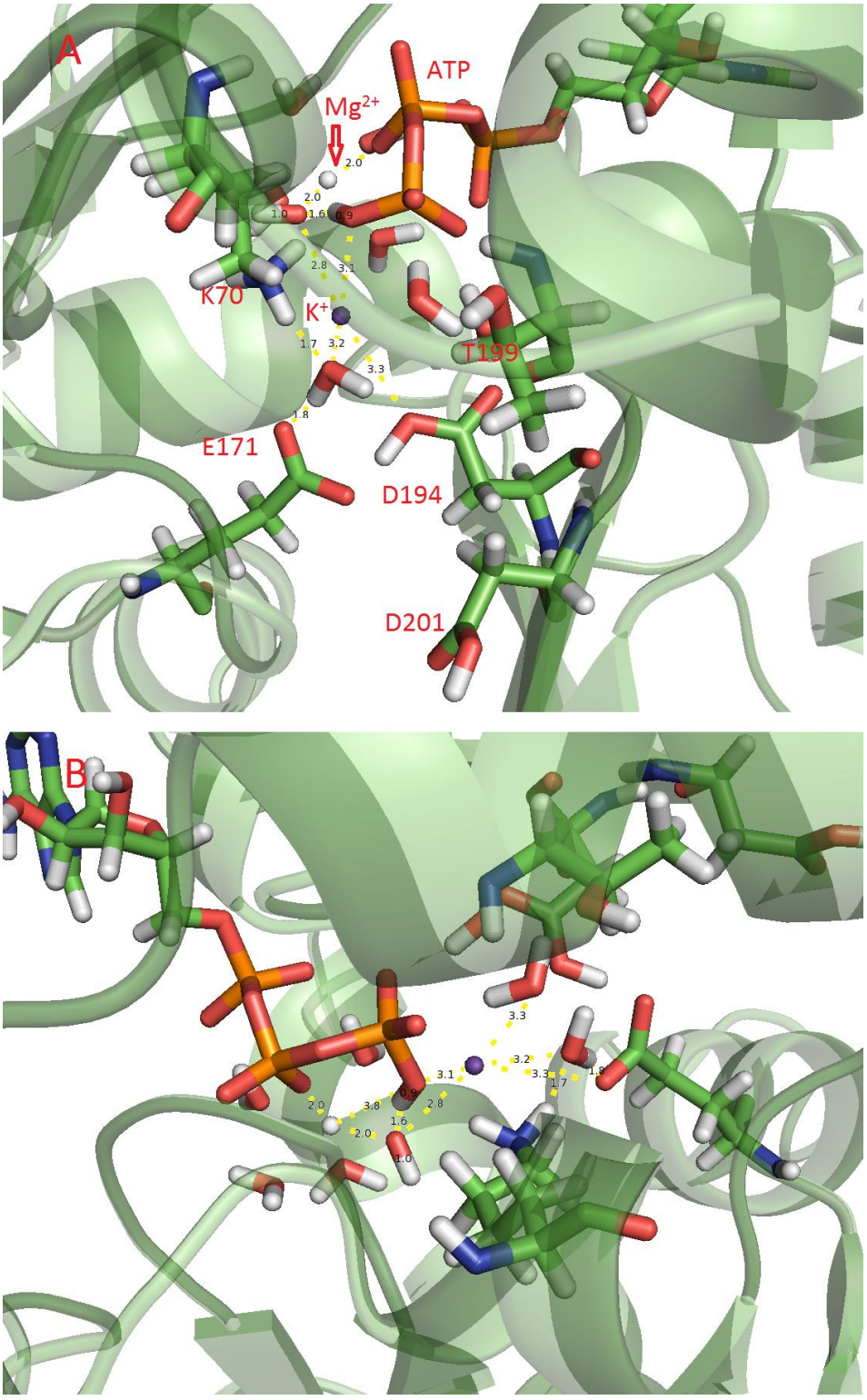

Figure 3.7 : The structure (**AcidWN**) obtained after the proton transfer from the water between Mg^{2+} and K^{+} to the γ-phosphate A) in the same orientation as Figure 3.1, B) in an orientation rotated by 90° with respect to (A) (the O-H distance has been frozen during optimization, distances in Å).

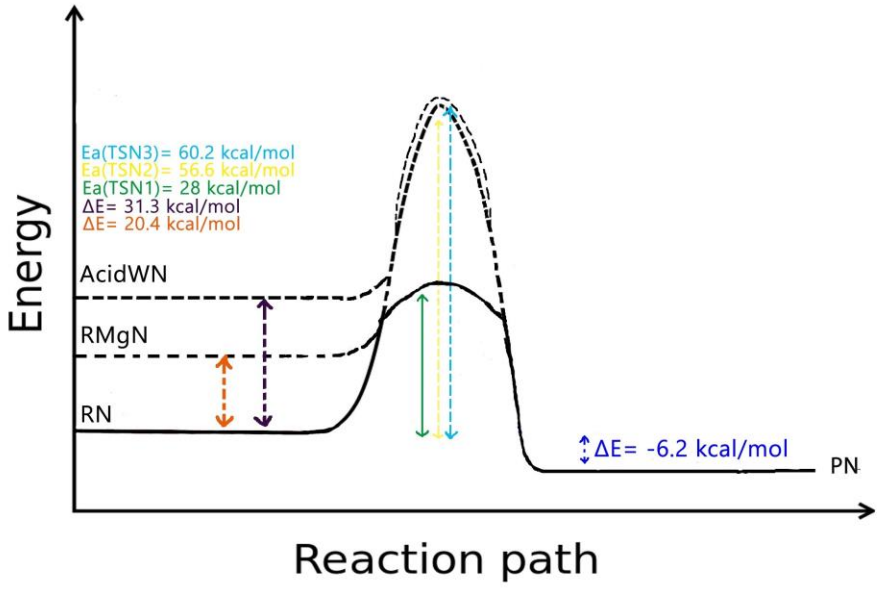

Figure 3.8 : Energy versus reaction path graph of the 201N models.

3.2 Hydrolysis in the 201I System

Several transitions structures and products have been optimized for the 201I system. Their energies relative to the most stable reactant structure are displayed in Table 3.2.

Table 3.2 : Relative energies (with respect to **RI**) of the stationary points in the reaction of 201I.

NAME	Relative energy (kcal/mol)
PI	9.8
P171I	11.8
P201I	11.8
CI	26

In the optimized reactant structure for the 201I model (**RI**), both T199 and D201 are in the active site. The nucleophilic water is between K70 and T199. T199 directly interacts with the γ-phosphate. K70 positions one of its H atoms next to the nucleophilic water instead of a water molecule solvating E171. The latter water molecule interacts with the nucleophilic water and forms an H-bond with D201 instead of D194. K^+ is also positioned differently than

in the 201N model. It interacts with D194, D201, ATP (2.7 Å) and to a lesser extent, T199. This structure has a second K^+ atom positioned at the α-phosphate (Figure 3.9).

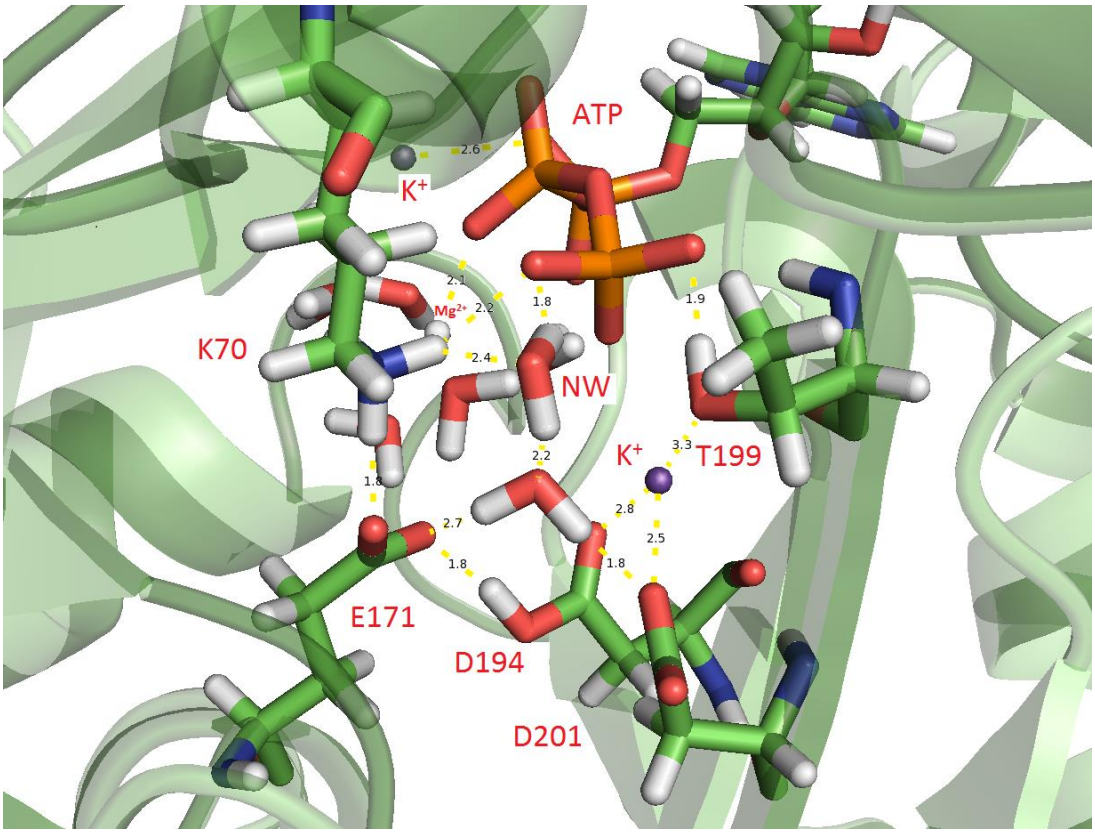

Figure 3.9 : The most stable reactant structure (**RI**) in the 201I system.

In the product structure of 201I model formed right after the hydrolysis (**PI**, Figure 3.10), interactions with K70 and T199 are stronger as a result of the Pi formation. Interaction between K70 and E171 is weakened by 0.1 Å and K^+ also shifted by 0.1 Å towards D194 and 0.1 Å away from D201. Relative energy of this structure with respect to the reference reactant is 9.8kcal/mol. This value will be exothermic when Pi completely leaves the protein. An interesting point in this geometry is the interaction of the Pi with the water between E171 and D194. The distance between Pi and this water molecule is 1.4 Å, and this water has stronger interactions with E171 and D194 than in **RI**. This led us to test the possibility of E171 or D201 accepting a proton from Pi through that water molecule.

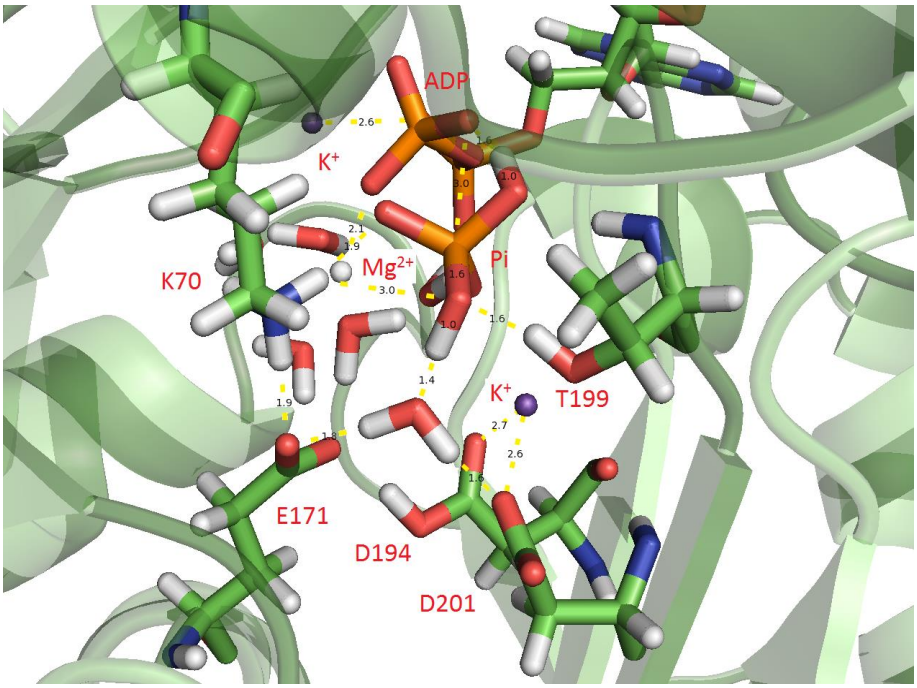

Figure 3.10 : The most stable product structure (**PI**) in the 201I system.

Product structure with E171 accepting a proton from the Pi resulted in further elongation of the cleaving bond by 0.2 Å and K70 having a stronger interaction with the Pi and a weaker interaction with E171 (**P171I**, Figure 3.11). K^+ shifted away from D194 by 0.1 Å. Relative energy for this structure is 11.8 kcal/mol, 2 kcal/mol higher than **PI** (Table 3.2).

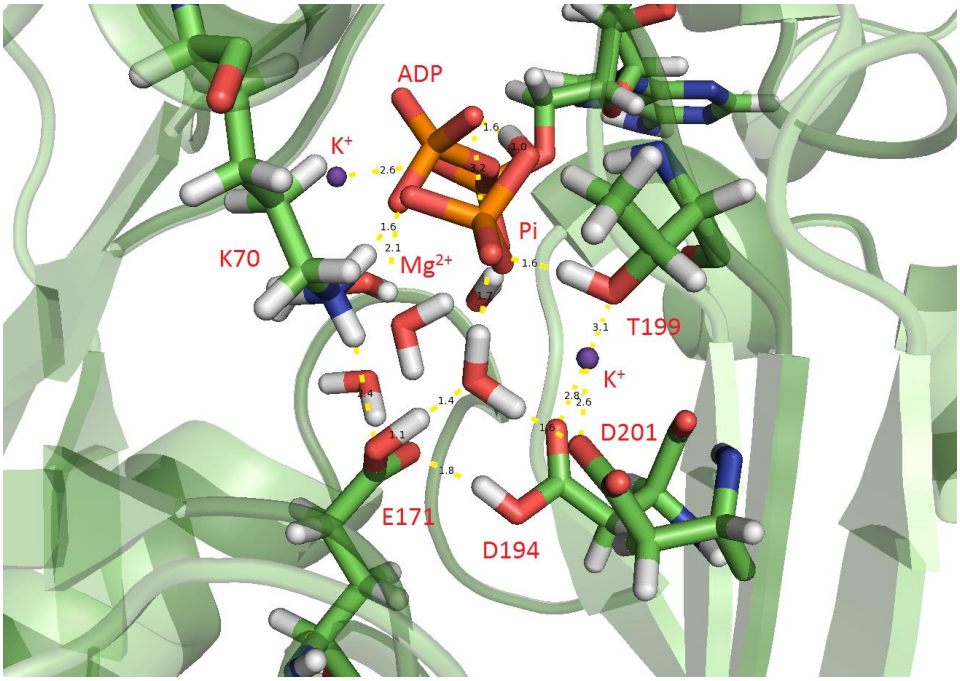

Figure 3.11 : The product with E171 accepting a proton from Pi (**P171I**).

Optimizations with D201 accepting a proton (**P201I**) resulted in the shift of the proton back to the water, creating a hydronium ion in the process (Figure 3.12). Relative energy for this structure is -11.8 kcal/mol. These optimizations led us to think that considering our results, the protonation of E171 may ocur after the completion of the ATP hydrolysis. Or the proton can pass on a water to form a hydronium ion. Both of these processes require only 2 kcal/mol and a slight change in the environment due to the linker or DnaJ may make them more favoravle. Proton donation by Pi increases the negative charge on it, resulting a higher electrostatic repulsion between ADP and Pi which would facilitate the release of Pi.

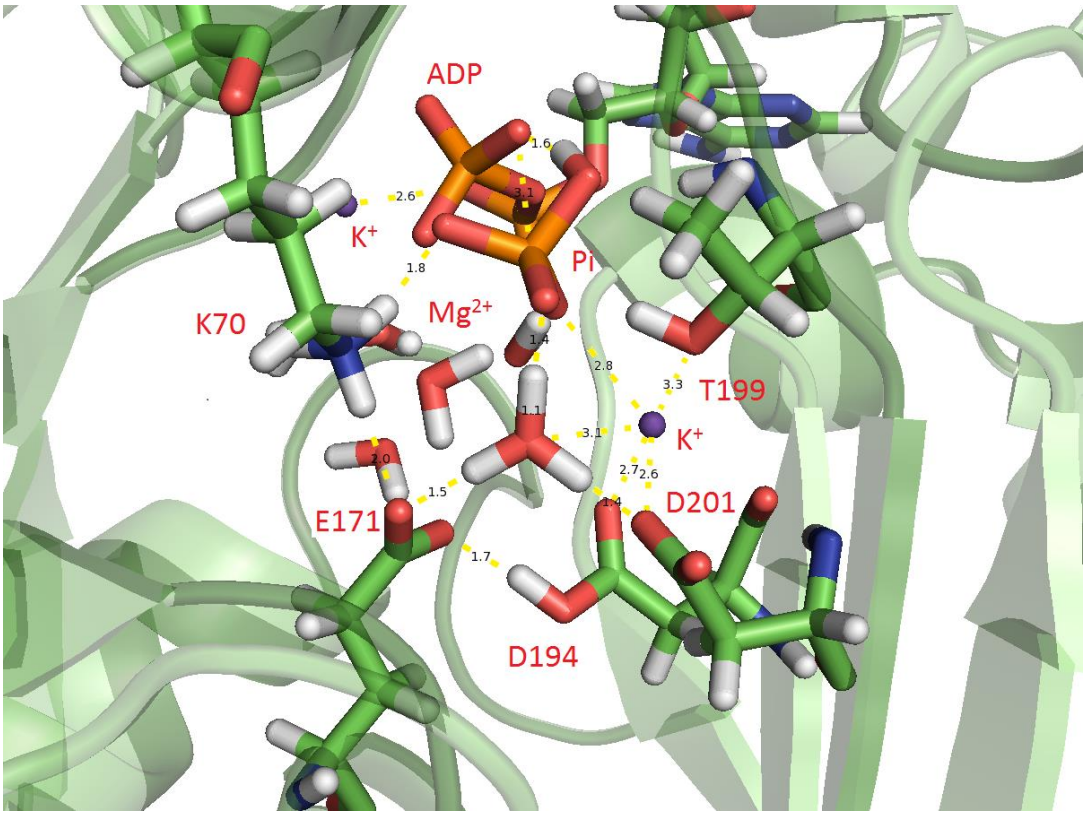

Figure 3.12 : The product with hydronium formation after D201 did not accept a proton from Pi (**P201I**).

Alternative geometries to test the initiation of the reaction by a shift in the Mg^{2+} position as suggested by McKay and coworkers have also been attempted in the 201I model. **RI** has been manually modified by putting Mg^{2+} between β- and γ-phosphates. But geometry optimizations resulted in Mg^{2+} shifted back to its original position. In addition, product structures with Mg^{2+} coordinated to β-phosphate and Pi (designed by manually modifying **PI** or **P171I**) to reproduce the crystals have failed, again Mg^{2+} shifting back to its original position. In another attempt to locate Mg^{2+}

between β- and Pi, the crystallographic ADP + Pi + Mg^{2+} configuration has been placed into **PI**. Coordination shell of the Mg^{2+} is then rearranged accordingly. In the optimized geometry (**CI**, Figure 3.13), Mg^{2+} remained between the two phosphate groups. K70 shifted away from E171 to Pi. There is a water molecule between the Pi and the ADP. The distance of the water between E171 and D201 is equal to both of the residues. Pi gives one of its H atoms to this water, creating hydronium. Relative energy for this structure is 26 kcal/mol. This much relative energy may be obtained because we tried to manually replace ATP+Mg^{2+} and the environment could not rearrange itself in this new geometry.

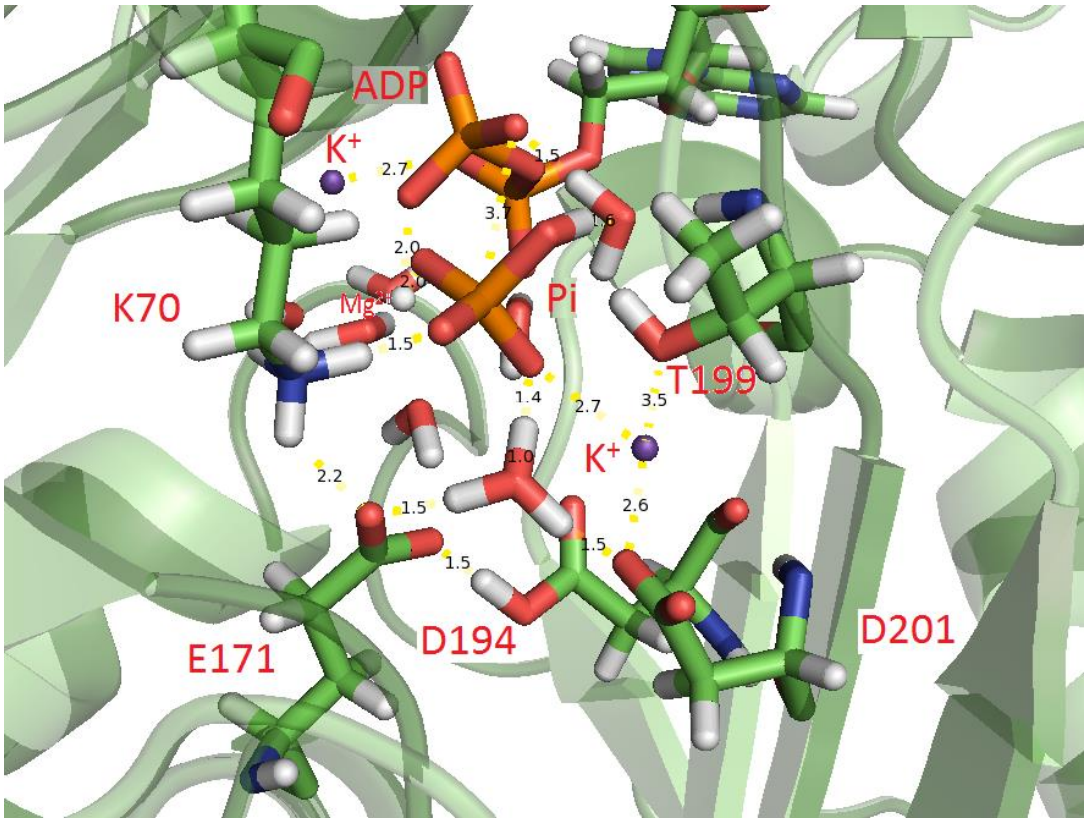

Figure 3.13 : Product structure with ATP+Mg obtained from crystal structure (**CI**).

After observing that the Pi has the ability to deprotonate, we considered the options with that donated proton completely leaving the active site and decided to try out models with deleting one proton from the Pi to understand the effect of the deprotonation of Pi.

Table 3.3 : Relative energies (With respect to PHI0) of the stationary points in the reaction of 201I.

NAME	Relative energy (kcal/mol)
PHI1	-3.2
PHI2	-4.2

Reference product (**PHI0**, Figure 3.14) for the studies with a deleted proton from the structure is created with Mg^{2+} coordinating only with the β-phosphate group. In this structure, K70 does not interact directly with E171 but has a H-bond with Pi. The water between E171 and D201 shows a weaker interaction to D201. K^+ shifted 0.1 Å away from D194. Cleaved phosphate bond is 0.2 Å longer than **PI**, but the H-bond between Pi and the ADP is 0.1 Å shorter.

Two models for the situation where Mg^{2+} is coordinated between the β-phoshphate and Pi have been created for this study. **PHI1** lacks the proton oriented away from ADP and **PHI2** does not have the proton interacting with ADP in the product structure. Both models have Mg^{2+} between β- and γ-phosphate groups. Coordination shells have been rearranged accordingly before calculations.

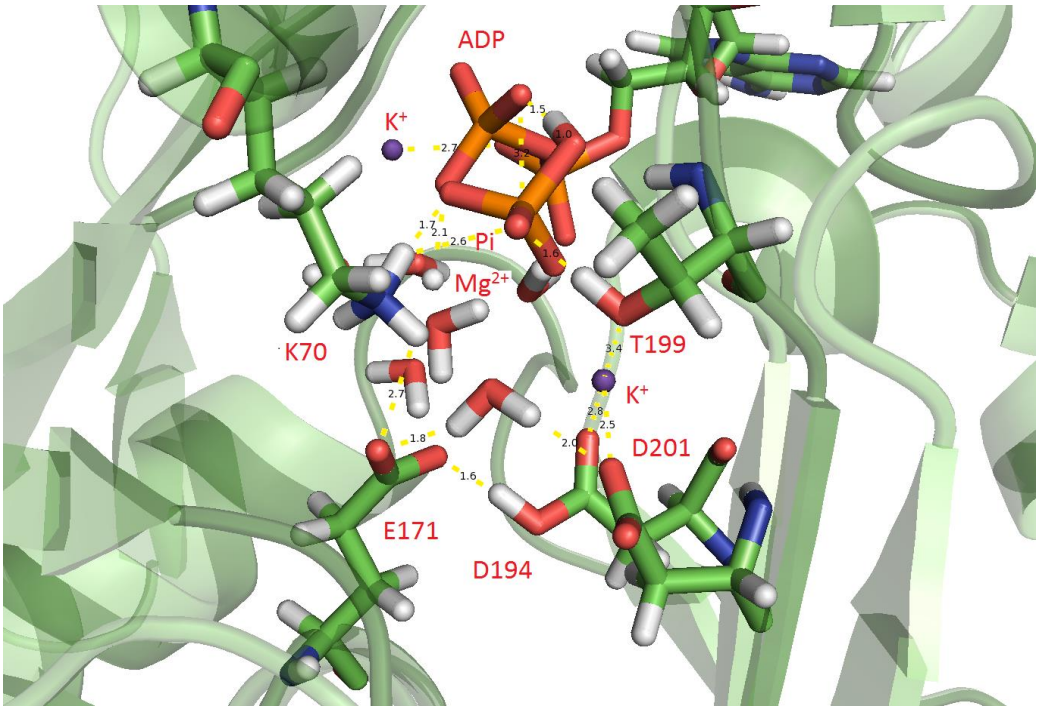

Figure 3.14 : Reference product with a deleted proton from Pi (**PHI0**).

First model (**PHI1**) has the same proton deleted as the reference structure (Figure 3.15). Mg^{2+} interacts with both β-phosphate and Pi. The distances of Pi from ADP, T199 and K70 are all longer by 0.1 Å with respect to **PHI0**. K70 is closer to E171 than the reference product structure by 0.8 Å. The water between E171 and D201 shifted towards D201. K^+ shifted towards T199 from D201 by 0.1 Å. Relative energy of this structure to the reference product is -3.2 kcal/mol.

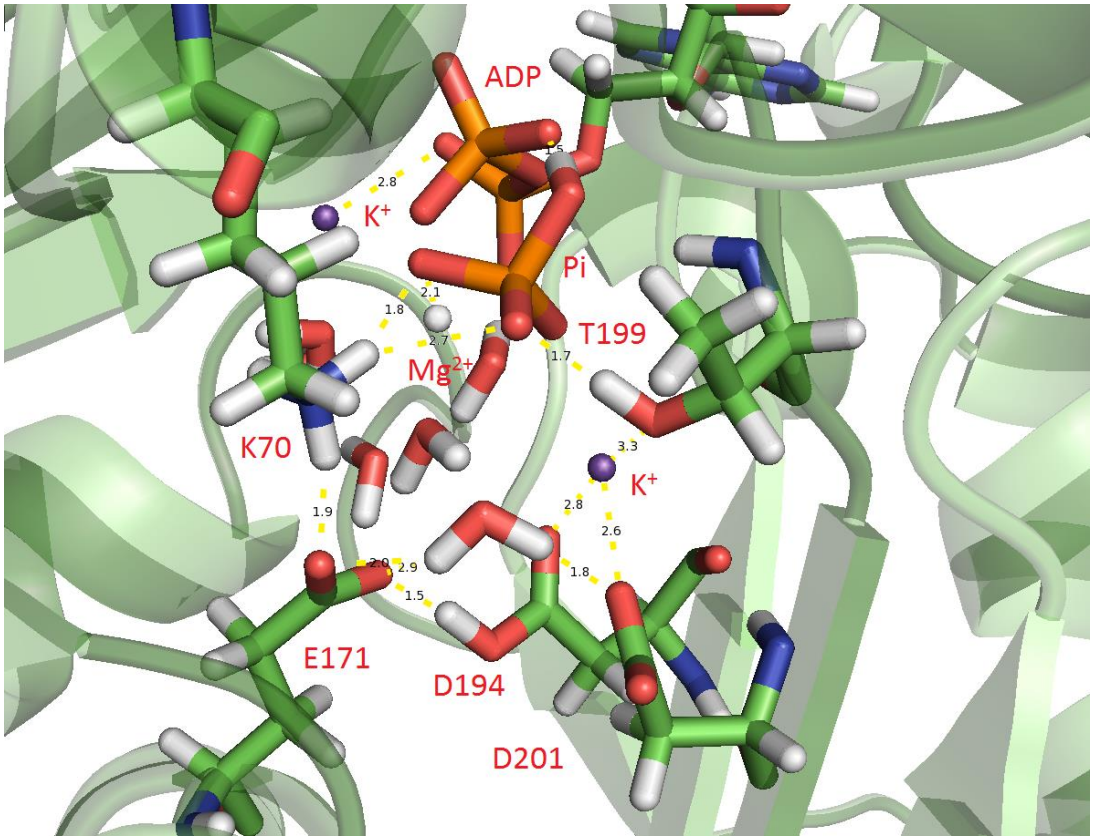

Figure 3.15 : Product structure with the proton facing towards a nearby water deleted on Pi (**PHI1**).

Proton facing ADP is removed in **PHI2**. Mg^{2+} interacts with both the b phosphate and Pi, but its coordination shell is arranged in a distorted octahedral manner (Figure 3.16). Unlike the crystallographic structure and **PHI1**, Mg^{2+} interacts with two O atoms of the Pi, one O atom of the ADP and three adjacent water molecules. Cleaved bond between β- and γ- phosphate group is 0.1 Å shorter from **PHI1** and 0.2 Å shorter from **PHI0**. K^+ is located as in **PHI0**. Orientation of the K70 is similar to the **PHI1**. D194 is very close to the E171. The water between E171 and D201 has equal distance to the both residues, forming an H bond with both of them. Pi strongly interacts with this water. Relative energy of this structure to the reference product is

-4.2 kcal/mol, meaning this structure is more energetically favorable even though it has a distorted coordination shell for Mg^{2+}.

These results indicate that the position of Mg^{2+} being between β-phosphate and Pi is energetically favorable only when Pi is deprotonated. With a more negatively charged Pi, it is possible that Mg^{2+} can shift towards Pi.

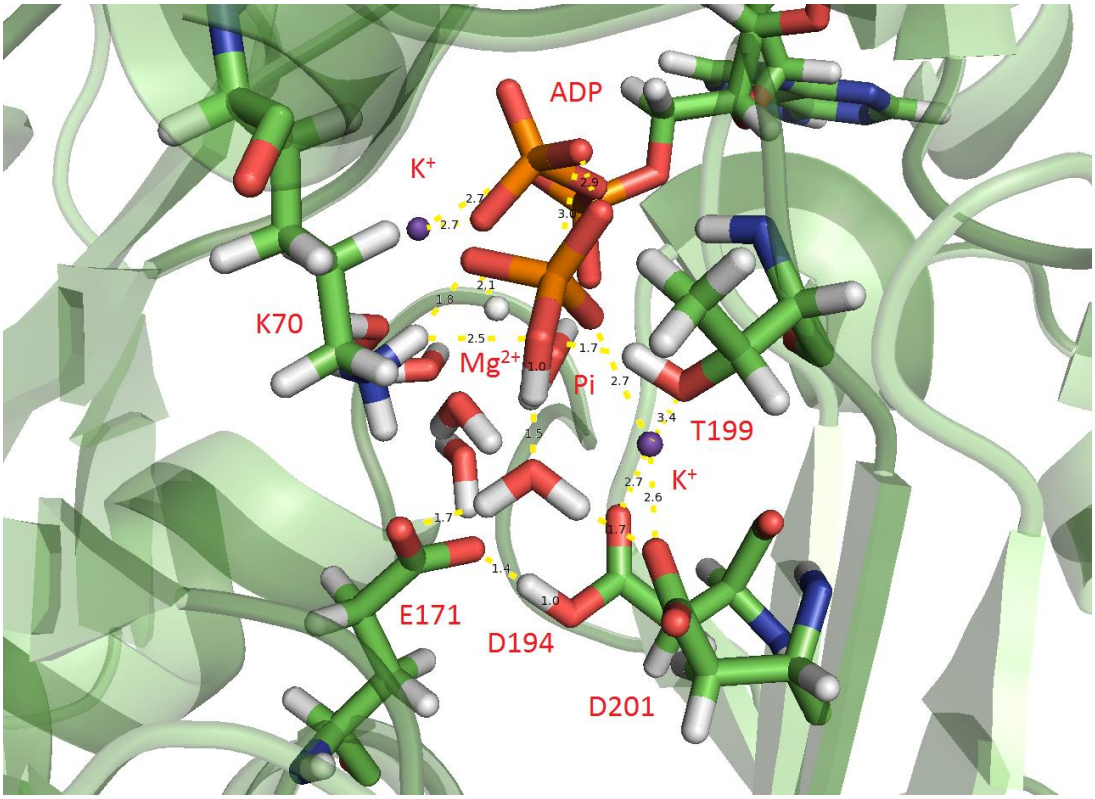

Figure 3.16 : Product structure with the proton facing ADP deleted on Pi (**PHI2**).

The mechanism involving a water molecule between Mg^{2+} and K^+ donating a proton to the γ-phosphate is also tested in the 201I model (Figure 3.17). We had the same problems in this calculation like in 201IN model, so the calculation was performed having a constraint between the donated proton and the acceptor O atom on the γ-phosphate. The biggest difference from the reactant structure is the reorientation of the nucleophilic water and K^+. K^+ shifted 0.9A away from T199, 0.2 Å away from D201 and 0.1 Å towards D194 compared to **RI**. Relative energy of this structure is 20.1 kcal/mol to the 201I reactant structure, which is also too high to be the initial step of a general acid catalyzed reaction.

The relative energies of all of our 201N models can be seen in the energy versus reaction path graph (Figure 3.18), where unlikely mechanisms are shown in dashed

lines. We could not optimize a transition state, so it is left blank. The models with a deleted proton on Pi are excluded from this graph, because only the models which have the same number and same type of atoms are energetically comparable.

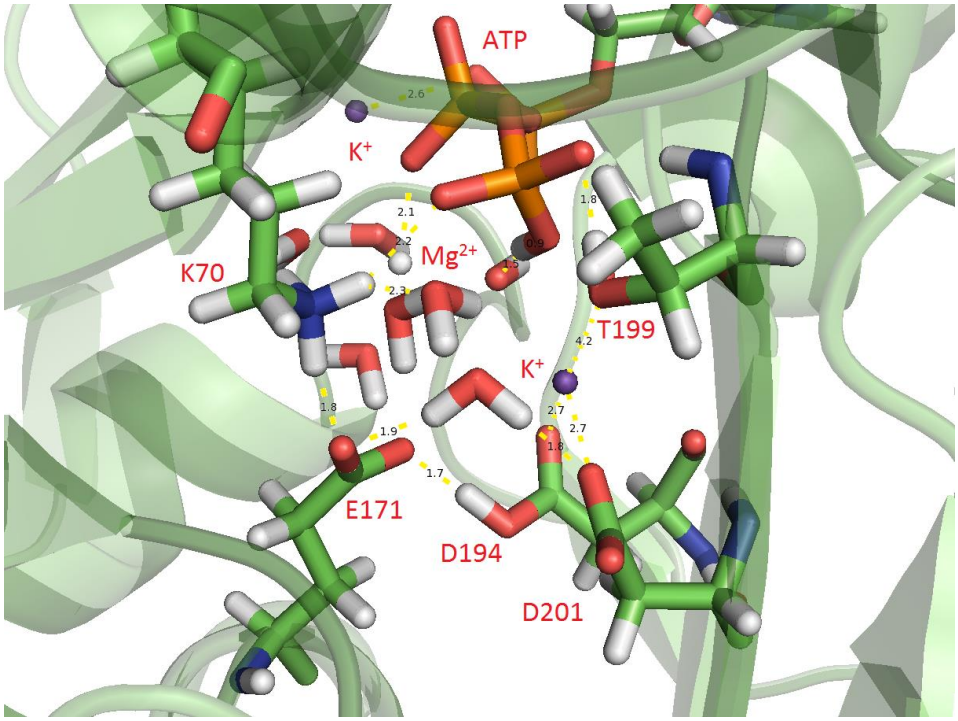

Figure 3.17 : The structure (**AcidWI**) obtained after the proton transfer from the water between Mg^{2+} and K^{+} to the γ-phosphate.

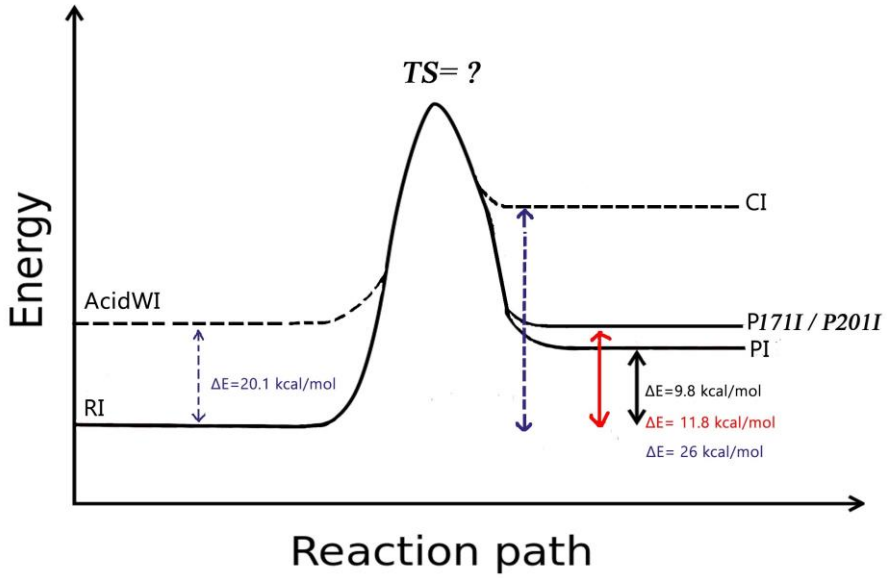

Figure 3.18 : Energy versus reaction path graph of the 201N models.

4. CONCLUSIONS AND RECOMMENDATIONS

This study analyzed the hydrolysis mechanism of the chaperone protein Hsp70. We tried to shed light on that if the reaction pathway is associative or dissociative, protonation states of the critical residues in the active site and if there is an acid-base catalysis or not with creating two different main models based on the protonation state of D201 (**201N** and **201I**). This choice has been made because of the orientations of the two critical residues D201 and T199. When D201 is protonated, it is oriented away from the active site and T199 does not interact with ATP. On the other hand, deprotonated D201 faces towards the active site and T199 directly interacts and creates a H-bond with ATP.

In the 201N structures, we observed that placing Mg^{2+} between β- and γ-phosphates gave an energetically unfavorable result for reaction initiation as previously suggested. In our transition structures, we considered E171 as a base candidate. Acid candidates were K70, D194, and a water molecule between Mg^{2+} and K^{+}. Three of those transition structures were succesful, with all of them having associative character, one with direct hydrolysis with the nucleophilic water without involment of any other residue, one with E171 as a base without an acid, and one with D194 as an acid with E171 as a base. Only the one with direct hydrolysis (**TSN1**) gave a result which can be considered consistent with experimental values. If K70 and T199 is involved in this reaction, one may obtain better results.

We tried to search for a dissociative transition state but those tests always resulted in going to the reactant or product states, so we can say that the reaction does not proceed via dissociative pathway.

The results with our other transition states led us to think that there is not an acid-base catalysis involved in the reaction mechanism, but the residues expected to participate an acid-base catalysis mechanism have other important roles in the active site.

In 201I models, we observed that Pi has a tendency to donate a proton to a nearby water molecule, creating a hydronium ion in the process. Alternatively, this proton can pass into E171. These two possibilities are energetically identical and requires 2 kcal/mol to occur after the product formation.

After the formation of hydronium, this hydronium can leave the environment. To mimic that, we created models with a deleted proton from Pi. After our initial model, we tried this model type with Mg^{2+} between β-phosphate and Pi. These calculations gave exothermic results with respect to our initial model which has Mg^{2+} only interacting the b position. This means that it is only energetically favorable for Mg^{2+} to be found between β-phosphate and Pi when Pi is deprotonated.

Overall, it is possible that the reaction is following an associative path with no acid-base catalysis and two key residues, K70 and T199 may assist stabilizing the transition structure. E171 (and possibly D194) retain its charge until after hydrolysis occurs and Pi forms. E171 may act as a base only after the product formation, receiving a proton from the Pi. Alternatively, Pi can donate a proton to a nearby water, creating a hydronium ion. With this behaviour, Pi can leave the environment relatively easily because the resulting negative charge on Pi can cause a stronger repulsion from ADP.

It is suggested that D194 has a role in Mg^{2+} binding. Deprotonation of D194 before product formation may cause disorientations in the active site. The pH profile studies can be explained with this, because when D194 is mutated into alanine, which is also a neutral residue, rate increases with increasing pH. The increasing rate with the pH is may be the result of the deprotonation of Pi and Pi leaving easily from the environment because of the deprotonation.

Particular attention should be paid to the protonation state of D194 in the reactant and product states and behaviour of this residue in respect to its protonation state. Another important points are the movement of Pi after product formation and Pi donating a proton to E171 or hydronium, all of which can be done via molecular dynamics simulations. For the QM part, options with T199 and K70 assisting the hydrolysis mechanism should be examined in detail.

REFERENCES

[1] **Mayer M.P., Bukau B.** (2004) Hsp70 Chaperones: Cellular Functions and Molecular Mechanism. *Cell. Mol. Life Sci*, **62**. 670–684

[2] **Swain J.F., Dinler G, Sivendran R, Montgomery D.L., Stotz M., Gierasch L.M.** (2007) Hsp70 Chaperone Ligands Control Domain Association via an Allosteric Mechanism Mediated by the Interdomain Linker *Molecular Cell* **26**. 27–39

[3] **Flaherty K.M., Wilbanks S.M., DeLuca-Flaherty C, McKay D.B.** (1994) Structural Basis of the 70-Kilodalton Heat Shock Cognate Protein ATP Hydrolytic Activity II. *The Journal of Biological Chemistry*, **269**. 12899-12907

[4] **Kityk, R., Kopp, J., Sinning, I., Mayer, M.P.** (2012) Structure and Dynamics of the ATP-Bound Open Conformation of Hsp70 Chaperones. *Mol.Cell* **48**: 863

[5] **Zhurlavleva A., Clerico E.M., Gierasch L.M.** (2012) An Interdomain Energetic Tug-of-War Creates the Allosterically Active State in Hsp70 Molecular Chaperones. *Cell* **151**. 1296-1307

[6] **Johnson, E.R., McKay D.B.** (1999) Mapping the role of active site residues for transducing an ATP-induced conformational change in the bovine 70-kDa heat shock cognate protein. *Biochemistry* **38**: 10823-18830

[7] **O'Brien, M.C., McKay D.B.** (1995) How Potassium Affects the Activity of the Molecular Chaperone Hsc70 I. *The Journal of Biological Chemistry*, **205**. No. 5. 2247-2250

[8] **Wilbanks, S.M., McKay D.B.** (1995) How Potassium Affects the Activity of the Molecular Chaperone Hsc70 I. *The Journal of Biological Chemistry*, **205**. No. 5. 2251-2257

[9] **Palleros D.R., Reid K.L., Shi L., Welch W.J., Fink A.L.**(1993) ATP-induced protein-Hsp70 complex dissociation requires K+ but not ATP hydrolysis. *Nature* **365**. 664-666

[10] **İmamoğlu R.** ATPase Domain of DnaK, Escherichia Coli Hsp70 Molecular Chaperone, Experiences pH-Dependent ATPase Activity Upon Linker Binding (M.Sc. Thesis). Adress: Istanbul Teknik Üniversitesi

[11] **Barthel T.K., Zhang J, Walker G.C.** (2001) ATPase-Defective Derivatives of Escherichia coli DnaK That Behave Differently with Respect to ATP-Induced Conformational Change and Peptide Release. *Journal of Bacteriology* **183**. No. 19 5482-5490

[12] **Sousa M.C., McKay D.B.** (1998) The Hydroxyl of Threonine 13 of the Bovine 70-kDa Heat Shock Cognate Protein Is Essential for Transducing the ATP-Induced Conformational Change. *Biochemistry*, **37**. 15392-15399

[13] **Wilbanks S.M., DeLuca-Flaherty C, McKay D.B.** (1994) Structural Basis of the 70-Kilodalton Heat Shock Cognate Protein ATP Hydrolytic Activity I. *The Journal of Biological Chemistry*, **269**. 12893-12899

[14] **Vogel M, Bukau B, Mayer M.P.** (2006) Allosteric Regulation of Hsp70 Chaperones by a Proline Switch. *Molecular Cell* 21, 359–367

[15] **Klähn M, Rosta E, Warshel A**.(2006) On the Mechanism of Hydrolysis of Phosphate Monoesters Dianions in Solutions and Proteins. *Journal of the American Chemical Society,* **128**. no.47,15310-15323.

[16] **Hoff, R. H., & Hengge, A. C.** (1998). Entropy and Enthalpy Contributions to Solvent Effects on Phosphate Monoester Solvolysis. The Importance of Entropy Effects in the Dissociative Transition State .*J. Org. Chem,* **63,** 6680-6688

[17] **Bianciotto, M., J. C. Barthelat and A. Vigroux**. (2002).Reactivity of Phosphate Monoester Monoanions in Aqueous Solution. 1. Quantum Mechanical Calculations Support the Existence of "Anionic Zwitterion" Meo(+)(H)Po(3)(2-) as a Key Intermediate in the Dissociative Hydrolysis of the Methyl Phosphate Anion, *J Am Chem Soc* **124**, no. 25,7573-7587

[18] **Kamerlin, Shina C. L., Jan Florián and Arieh Warshel**.(2008). Associative Versus Dissociative Mechanisms of Phosphate Monoester Hydrolysis: On the Interpretation of Activation Entropies, *ChemPhysChem* **9**, no. 12, 1767-1773.

[19] **Maegley, K A, S J Admiraal and D Herschlag**. (1996).Ras-Catalyzed Hydrolysis of Gtp: A New Perspective from Model Studies, *Proceedings of the National Academy of Sciences* **93**, no. 16, 8160-8166.

[20] **Lassila, J. K., J. G. Zalatan and D. Herschlag**. (2011). Biological Phosphoryl-Transfer Reactions: Understanding Mechanism and Catalysis, *Annu Rev Biochem,* **80**, 669-702

[21] **Florián, Jan, Johan Åqvist and Arieh Warshe**l. (1998).On the Reactivity of Phosphate Monoester Dianions in Aqueous Solution: Brønsted Linear Free-Energy Relationships Do Not Have an Unique Mechanistic Interpretation, *Journal of the American Chemical Soc*iety, **120**, no. 44,11524-11525.

[22] **Kamerlin, Shina C. L., Jan Florián and Arieh Warshel**.(2008). Associative Versus Dissociative Mechanisms of Phosphate Monoester Hydrolysis: On the Interpretation of Activation Entropies, *ChemPhysChem* **9**, no. 12, 1767-1773.

[23] **Cleland, W.W. & Hengge, A. C**. (2006). Enzymatic mechanisms of phosphate and sulfate transfer. *Chemical Reviews* **106**, 3252–3278

[24] **Aqvist, J., K. Kolmodin, J. Florian and A. Warshel**. (1999). Mechanistic Alternatives in Phosphate Monoester Hydrolysis: What Conclusions Can Be Drawn from Available Experimental Data?, *Chem Biol* **6**, no. 3,R71-80.

[25] **Boero M, Ikeda T, Etsuro I, Terakura K.** (2006) Hsc70 ATPase: An Insight into Water Dissociation and Joint Catalytic Role of K+ and Mg2+ Metal Cations in the Hydrolysis Reaction. *J. Am. Chem. Soc.* 128, 16798-16807.

[26] **Vreven T., Morokuma K., Farkas Ö, Schlegel H.B., FRISCH M. J.** (2003).Geometry optimization with QM/MM, ONIOM, and other combined methods. I. Microiterations and constraints. *J Comput Chem*. **24,** no. 6,760-769.

[27] **Senn HM., Thiel W.**, .(2009). QM/MM methods for biomolecular systems. *Angew Chem Int Ed Engl*. **48**, no.7,1198-1229

[28] **C. F. Matta** (Ed.) (2010) Quantum Biochemistry: Electronic Structure and Biological Activity, Wiley-VCH, Weinheim.

[29] **Gaussian 09, Revision A.02,** M. J. Frisch, G. W. Trucks, H. B. Schlegel, G. E. Scuseria, M. A. Robb, J. R. Cheeseman, G. Scalmani, V. Barone, B. Mennucci, G. A. Petersson, H. Nakatsuji, M. Caricato, X. Li, H. P. Hratchian, A. F. Izmaylov, J. Bloino, G. Zheng, J. L. Sonnenberg, M. Hada, M. Ehara, K. Toyota, R. Fukuda, J. Hasegawa, M. Ishida, T. Nakajima, Y. Honda, O. Kitao, H. Nakai, T. Vreven, J. A. Montgomery, Jr., J. E. Peralta, F. Ogliaro, M. Bearpark, J. J. Heyd, E. Brothers, K. N. Kudin, V. N. Staroverov, R. Kobayashi, J. Normand, K. Raghavachari, A. Rendell, J. C. Burant, S. S. Iyengar, J. Tomasi, M. Cossi, N. Rega, J. M. Millam, M. Klene, J. E. Knox, J. B. Cross, V. Bakken, C. Adamo, J. Jaramillo, R. Gomperts, R. E. Stratmann, O. Yazyev, A. J. Austin, R. Cammi, C. Pomelli, J. W. Ochterski, R. L. Martin, K. Morokuma, V. G. Zakrzewski, G. A. Voth, P. Salvador, J. J. Dannenberg, S. Dapprich, A. D. Daniels, O. Farkas, J. B. Foresman, J. V. Ortiz, J. Cioslowski, and D. J. Fox, Gaussian, Inc., Wallingford CT, 2009.

[30] **AMBER 10,** D.A. Case TAD, T.E. Cheatham, III, C.L. Simmerling, J. Wang, R.E. Duke, R. Luo,, M. Crowley RCW, W. Zhang, K.M. Merz, B.Wang, S. Hayik, A. Roitberg, G. Seabra, I., Kolossváry KFW, F. Paesani, J. Vanicek, X.Wu, S.R. Brozell, T. Steinbrecher, H. Gohlke,, L. Yang CT, J. Mongan, V. Hornak, G. Cui, D.H. Mathews, M.G. Seetin, C. Sagui, V. Babin,, Kollman:, University of California, San Francisco. 2008.

[31] **Froresman. J. B., and Frisch. Æ.** (1993). Exploring Chemistry with Electronic Structure Methods, Second Edition. U. S. A.: Gaussian, Inc.

[32] **Frisch, Æ., and Frisch, M. J**. (1999). Gaussian 98 User's Reference, Second Edition. U. S. A.: Gaussian, Inc.

[33] **Christopher J. Cramer.** (2004), Essentials of Computational Chemistry: Theories and Models, Second Edition, John Wiley & Sons

[34] **Andrew R. Leach** (1996) Molecular Modelling Principles and Applications Second Edition, Prentice Hall.

[35] **Zhao Y., Truhlar D. G.** (2008). The M06 suite of density functionals for main group thermochemistry, thermochemical kinetics, noncovalent interactions, excited states, and transition elements: two new functionals and systematic testing of four M06-class functionals and 12 other functionals. *Theor. Chem Account.* **120**, 215–241.

[36] **Dunning, T. H.**(1989).Gaussian basis sets for use in correlated molecula calculations. I. The atoms boron through neon and hydrogen. *J.Chem. Phys*. **90**, 1007.

[37] **Zhao Y., Schultz N. E., Truhlar D. G.** (2006). Design of Density Functionals by Combining the Method of Constraint Satisfaction with Parametrization for Thermochemistry, Thermochemical Kinetics, and Noncovalent Interactions .*J. Chem. Theory Comput*, **2**, 364-382.

[38] **Zhao Y., Truhlar D. G**. (2006). A new local density functional for main-group thermochemistry, transition metal bonding, thermochemical kinetics, and noncovalent interactions.*J. Chem. Phys*. **125**,194101

[39] **Feller D.(1996).** The role of databases in support of computational chemistry calculations. *Journal of Computational Chemistry,* **17***,* no. 13, 1571-1586.

[40] **Vreven T., Morokuma, K, Farkas, O, Schlegel, H. B. Frisch, M. J.** (2006). Combining Quantum Mechanics Methods with Molecular Mechanics Methods in ONIOM , *Chem. Theory Comput*. 2, 815-826

[41] **Cornell W., Piotr Cieplak, Christopher I. Bayly, Ian R. Gould, Kenneth M. Merz, David M. Ferguson, David C. Spellmeyer, Thomas Fox, James W. Caldwell and Peter A. Kollman**.(1995).A Second Generation Force Field for the Simulation of Proteins, Nucleic Acids, and Organic Molecules, *J. Am. Chem. Soc.* **117**, no. 19, 5179–5197

[42] **Duan, Y., Wu, S. Chowdhury, M. C. Lee, G. Xiong, W. Zhang, R. Yang, P. Cieplak, R. Luo, T. Lee, J. Caldwell, J. Wang and P. Kollman**.(2003) A point-charge force field for molecular mechanics simulations of proteins based on condensed-phase quantum mechanical calculations, *J. Comput. Chem*., **24**, no. 16, 1999–2012

[43] **Foster JP, Weinhold F**.(1980) Natural hybrid orbitals. *Journal of the American Chemical Society,* **102***,* no.24, 7211-7218.

CURRICULUM VITAE

Name Surname **:** Oğuzhan MARABA

Date and Place of Birth **:** Istanbul, 29/05/1991

E-Mail **:** maraba@itu.edu.tr

EDUCATION:

- **B.Sc.** **:** 2009, Ege University, Faculty of Science, Biochemistry